Climate Dynamics (2023) 60:1963–1985
https://doi.org/10.1007/s00382-022-06417-8

Salinity interdecadal variability in the western equatorial Pacific and its effects during 1950–2018

Rong-Hua Zhang[1,2,3,4] · Guanghui Zhou[2,3] · Hai Zhi[5] · Chuan Gao[2,3,4] · Hongna Wang[2,4] · Licheng Feng[6]

Received: 20 August 2021 / Accepted: 4 July 2022 / Published online: 1 August 2022

Abstract

Ocean reanalysis products are used to examine salinity variability and its relationships with temperature in the western equatorial Pacific during 1950–2018. An ensemble empirical mode decomposition (EEMD) method is adopted to separate salinity and temperature signals at different time scales; a focus is placed on interdecadal component in this study. Pronounced interdecadal variations in salinity are seen in the region, which exhibits persistent and transitional phases in association with temperature. A surface freshening is accompanied by a surface warming during the 1980s and 1990s, but saltening and cooling in the 2000s, with interdecadal shifts occurring around in the late 1970s, late 1990s, and during 2016–2018, respectively. Determined by anomaly signs of temperature and salinity, their combined effects can be density-compensated or density-uncompensated, correspondingly acting to produce density variability that is suppressed or enhanced, respectively. The temperature and salinity effects are phase- and depth-dependent. In the subsurface layers at 200 m, where salinity and temperature anomalies tend to be nearly of the same sign during interdecadal evolution, their effects are mostly density-compensated. The situation is more complicated in the surface layer, where variations in sea surface salinity (SSS) and sea surface temperature (SST) exhibit different signs during interdecadal evolution. SST and SSS tend to be of opposite sign during the persistent phases with their effects being density-uncompensated; but they can be of the same sign during the transitional periods and the corresponding changes in SST and SSS undergo density-compensated relationships. Examples are given for the relationships among these fields which exhibit phase differences in sign transitions in the late 1990s; salinity effects are seen to cause a delay in phase transition of density anomalies. Furthermore, the relative contributions to interdecadal variabilities of density and stratification are quantified. The consequences of interdecadal salinity variability are also discussed in terms of their effects on local SST.

Keywords The western equatorial Pacific · Salinity interdecadal variability · Compensated and uncompensated effects · Relative contributions · EEMD method

✉ Rong-Hua Zhang
rzhang@qdio.ac.cn

[1] School of Marine Sciences, Nanjing University of Information Science and Technology, Nanjing 210044, China

[2] Key Laboratory of Ocean Circulation and Waves, Institute of Oceanology, and Center for Ocean Mega-Science, Chinese Academy of Sciences, Qingdao 266071, China

[3] University of Chinese Academy of Sciences, Beijing 10029, China

[4] Laboratory for Ocean and Climate Dynamics, Pilot National Laboratory for Marine Science and Technology, Qingdao 266237, China

[5] School of Atmospheric Sciences, Nanjing University of Information Science and Technology, Nanjing 210044, China

[6] National Marine Environmental Forecasting Center, Ministry of Natural Resources, Beijing 100081, China

1 Introduction

The western equatorial Pacific is a climatically important region where pronounced climate signals emerge at various time scales (e. g., Maes et al. 2006; Picaut et al. 1996; Feng et al. 2020). The warmest water pool is located in the region, where temperature exhibits variability at interannual and interdecadal scales associated with major climate modes, including El Niño-Southern Oscillation (ENSO) and Pacific Decadal Oscillation (PDO). Interannually in response to ENSO, for example, the warm waters in the western Pacific migrate eastward along the equator during El Niño but retreat westward during La Niña (Delcroix 1998; Lukas and Lindstrom 1991; Zhang et al. 2022). Historically, temperature (thermal) fields have been extensively used to investigate ENSO-related interannual variations for theoretical analyses and numerical modeling.

Salinity is another important variable in the ocean, which is a good indicator for climate variability and predictability (Miller 1976; Lukas and Lindstrom 1991; Maes et al. 2006; Li et al. 2013; Qu et al. 2014; Kang et al. 2014, 2017; Hu and Sprintall 2016; Guan et al. 2019; Du et al. 2019; Qi et al. 2019; Gao et al. 2020). For example, some notable salinity-related features emerge in the western equatorial Pacific, where fresh waters coexist with the warmest water pool. Climatologically, low salinity waters are found in the far western equatorial Pacific, whereas in the central basin near the date line, saline waters are generated by less freshwater inputs into the ocean at the ocean–atmosphere interface, thus producing a strong salinity front between the western and central equatorial Pacific. Variability of the low-salinity waters in the region is also closely related with the major climate modes (ENSO and PDO). For instance, interannual freshening and saltening take place in the western-central equatorial Pacific in association with ENSO (Picaut et al. 1996; Delcroix and Picaut 1998; Hasson et al. 2013; Gao et al. 2014). As observed (see Delcroix et al. 2011), both positive and negative sea surface salinity (SSS) anomalies can be found in the western tropical Pacific during El Niño events, with a freshening in the western equatorial Pacific and a saltening in the south-west tropical Pacific, respectively.

Temperature and salinity collectively determine ocean density, an important field to ocean pressure field and circulation. Depending on their relative contributions to density, the effects of temperature and salinity can give rise to different consequence for density anomalies. For example, when salinity and temperature anomalies are of the opposite sign, their combined net effects lead to enhanced density anomalies (i. e., density-uncompensated effect). In contrast, when they are of the same sign, their combined effects tend to be canceled out by each other (i. e., density-compensated), leading to density anomalies that are suppressed. The concept of spiciness has been introduced to represent density-compensated temperature and salinity variations with warm (cool) and salty (fresh) waters having high (low) spiciness (e.g. Schneider et al. 2000; Sasaki et al. 2010; Zhou and Zhang 2022). Furthermore, it is conceivable that in the density-compensated situation, the sign and amplitude of density anomalies can be even determined by salinity anomalies if its effects are greater than those of temperature.

As observed, pronounced salinity and temperature anomalies coexist in the tropical Pacific on different time scales (Zhang and Liu 1999; Cravatte et al. 2009), exhibiting their complicated interplays at different scales. On one hand, temperature and salinity anomalies are closely associated with the major climate modes in the region (Zhang and Busalacchi 2009; Zheng and Zhang 2012). So, their variabilities are seen to have a well-defined and coherent relationship. On the other hand, temperature and salinity are actually two different fields which are associated with different forcing, feedback effects, and the underlying processes and mechanisms. For example, these two fields exhibit different interannual characteristics and effects on density, which are strongly regionally dependent in the tropical Pacific. Associated with a direct forcing due to freshwater flux, for instance, large interannual variability region with SSS is located in the western equatorial Pacific. In contrast, large interannual variability of sea surface temperature (SST), directly affected by heat flux forcing, is located in the central and eastern equatorial basin. As a result, the way ocean density and pressure is affected by salinity and temperature is sensitively dependent on regions. In particular, because the effect of salinity in the western equatorial Pacific can have comparable magnitude to that of temperature, salinity can equally make contributions to density variability; but in the eastern equatorial Pacific, the effects of temperature largely dominate density variability. So, it is critically important to understand the characteristics of salinity variability, temperature–salinity (T–S) relationships and their combined net effects on density and resultant consequences.

Previously, temperature variability and its effects on density have received extensive attention. Due to the difficulty in observations, salinity variability and its effects have been less investigated; its roles in the ocean circulation and climate variability are less understood. As salinity observations and related reanalysis products become available (Delcroix et al. 2011), salinity variability and its relationships with temperature and other related fields have been examined in the tropical Pacific. On inter-annual time scales, for example, the extent to which salinity can play a role in determining density variability and barrier layer effects has been illustrated (Vialard et al. 2002; Zhang and Busalacchi 2009; Zhang et al. 2010;

Singh et al. 2011; Zhang et al. 2012; Zheng and Zhang 2012, 2015; Vinogradova and Ponte 2013; Zhu et al. 2014). On interdecadal scales, large salinity anomalies also coexist with temperature in the western equatorial Pacific, but its relationship with temperature and effects on density have not been clearly illustrated.

In this study, salinity variability and its effects on density in the western equatorial Pacific are analyzed using historical ocean reanalysis data. As seen, salinity variability exhibits its multiple scale signals in the tropical Pacific. To separate various components at different time scales, the ensemble empirical mode decomposition (EEMD) method is first used to extract different frequency components (Wu et al. 2007). Then, signals with specific frequency bands can be reconstructed. In this study, a focus is placed on salinity interdecadal variability in the western equatorial Pacific and its relationships with temperature and other derived fields. Relative contributions of temperature and salinity anomalies to anomalies of density and other related fields in the upper ocean are quantified to demonstrate their roles played in producing variabilities of density and vertical stratification (as represented by Brunt-Väisälä frequency, denoted as N^2).

The paper is organized as follows. Section 2 describes the methodology and dataset used in this study. Section 3 provides a brief description of the EEMD method that is used to extract signals at different time scales. Section 4 analyzes the effects on density, followed by relative contribution analyses in Sect. 5. Section 6 gives the conclusion and discussion.

2 Reanalysis data used

Ocean reanalysis products are used to illustrate salinity variability and its relationships with temperature in the tropical Pacific. Ocean salinity and temperature monthly fields are available from the ensembles (EN)_4.2.1.q ocean data product (1901-present) provided by the Met Office Hadley Center (Good et al. 2013), which cover the global ocean with horizontal resolution of $1° \times 1°$ and vertical depths from 5 to 5000 m.

Furthermore, some additional oceanic fields are diagnosed using the three-dimensional salinity and temperature fields, including potential density (hereafter it is simply referred as density), N^2, and the mixed layer (ML) depth (MLD). The TEOS-10 routine using the GSW V2.0 library (McDougall et al. 2012) is taken to calculate density (i.e., relative to the sea surface) and N^2. The MLD is calculated using a threshold method with a fixed density criterion (e.g., Maes 2000), in which the depth of ML is defined as the depth where the ocean density increases to 0.125 kg m^{-3} relative to that at the ocean surface. Note that potential density is referred to the density that a parcel would have if it were moved adiabatically to a chosen reference pressure, say, relative to the sea surface. If the reference pressure is chosen as the sea surface, then we first compute the potential temperature of the parcel relative to surface pressure, and then evaluate the density at pressure 0 dbar.

Figure 1a shows the climatological SSS distribution calculated from the reanalysis product during 1942–2018. Some well-known features include low SSS regions in the western equatorial Pacific, with a strong salinity front near the date line; so low-salinity waters coexist with warm waters in the far western equatorial Pacific. In terms of variations, interannual salinity variability is closely associated with ENSO cycles, characterized by zonal displacement of the fresh pool along the equator in the western tropical Pacific. The corresponding climatological SST distribution calculated from the reanalysis product during 1942–2018 is shown in the appendix (Fig. 15).

The seasonally-varying climatological fields for temperature and salinity (denoted as T_{clim} and S_{clim}) are also calculated during the periods 1942–2018. Then, their corresponding total interannual anomalies (denoted as T' and S') are obtained relative to the seasonally-varying climatological fields, with which the total fields can be written as $T = T_{clim} + T'$ and $S = S_{clim} + S'$. Figure 1b shows the horizontal distribution of the standard deviation (STD) for total interannual SSS anomalies in the tropical Pacific; the corresponding one for total interannual SST anomalies is shown in the appendix (Fig. 15). Interannual salinity variability is closely associated with ENSO cycles, characterized by zonal displacement of the fresh pool along the equator in the western tropical Pacific. Low-salinity fronts migrate eastward during El Niño but retreat westward during La Niña. So, large SSS variability center is located in the western equatorial Pacific, largely reflecting the zonal displacement of the salinity front. Another large SSS variability region is also found in the eastern equatorial Pacific. Note that there are important differences between Fig. 1b and the ENSO-related SSS anomalies extracted from in situ SSS data as presented in Delcroix et al. (2011). Possible reasons for such differences include different data sources and different periods analyzed. For example, the study of Delcroix et al. (2011) mainly used buoy and merchant ship-based observations which indicate geographically dependent uncertainties as seen in their sample length estimate (Fig. 2 in Delcroix et al. (2011)). Besides, the analysis periods are apparently different: the time period analyzed in Delcroix et al. (2011) is in 1970–2003, which is relatively short compared with ours in this study (1942–2018).

The original time series of the total interannual anomalies for salinity, temperature and density in the region A (6° S-4° N, 150° E–180°) in the western equatorial Pacific are shown

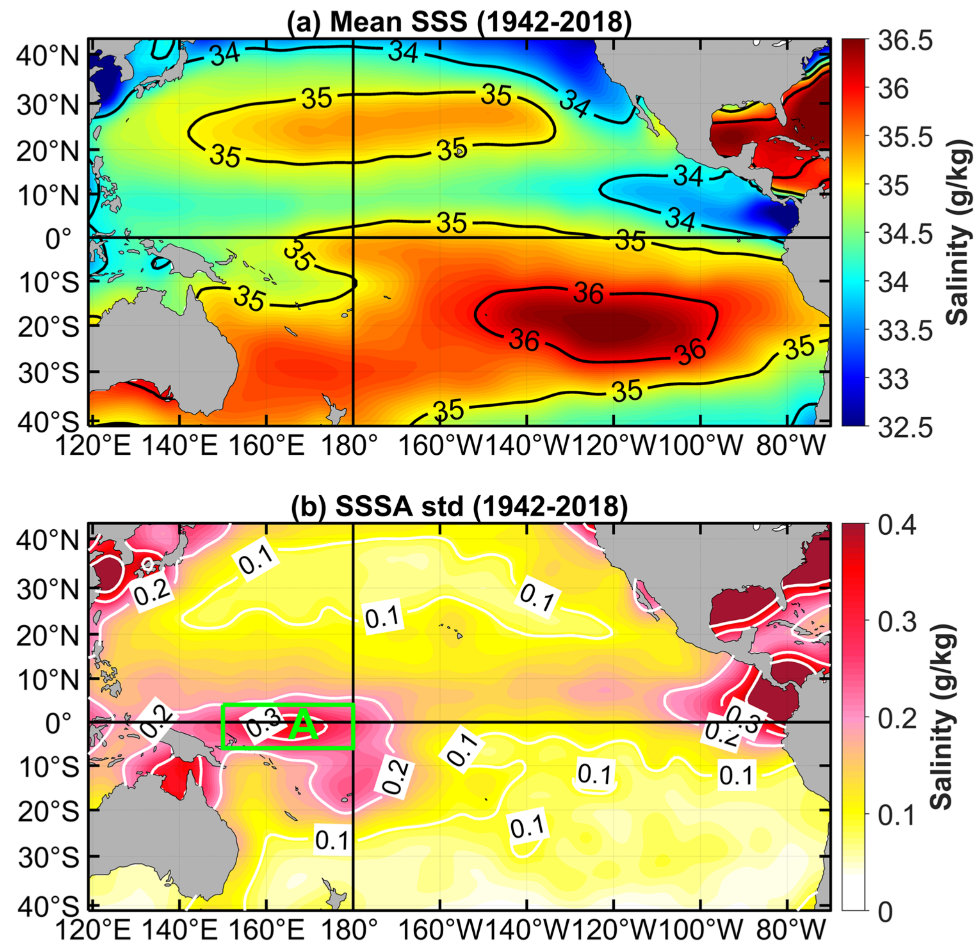

Fig. 1 Horizontal distribution of (a) climatological SSS field and (b) the standard deviation (STD) for SSS interannual fields in the tropical Pacific, which is calculated from the reanalysis data during the period 1942–2018. The green line denotes the focused analysis region (**A**) in this study: the western equatorial Pacific region (6° S–4° N, 150° E–180°), where a spatially averaged value for a field of interest is obtained accordingly. The unit is g kg^{-1}

in Fig. 2 during the period 1942–2018. Multiple-scale signals coexist, which reflect the major climate modes in the region, including ENSO and PDO. A well-defined relationship can be seen among these anomalies. For example, in the surface layer (Fig. 2a), SST and SSS anomalies are largely of the opposite sign, with their effects on sea surface density (SSD) tending to be uncompensated for by each other. The effects of SSS and SST anomalies on density are comparable in the region, and so salinity can play an important role in density variability. In subsurface layers, say at the depth of 200 m (Fig. 2b), temperature and salinity anomalies are nearly of the same sign, and their effects are thus density-compensated. Indeed, variations in density follow closely those of temperature, indicating that temperature anomalies are the dominant contributor to density variability. The visual impression of the opposite/same-sign relationships is confirmed by calculating the corresponding correlation coefficients between anomalies of SST and SSS and between those of subsurface temperature and salinity in the region A (Fig. 16 in the appendix); the former is about − 0.5 (Fig. 16a) and the latter is about 0.87 (Fig. 16b), respectively. Also, the relationships between density and temperature/salinity and their correlation coefficients are presented in the appendix (Fig. 17). Note that the effects of temperature and salinity are only very partially density-compensated; an estimate of compensation effects by temperature and salinity are given in the appendix (Fig. 18).

Note that the reanalysis shown in Fig. 2b is obviously not exploitable until at least around 1950 when the time series begins to show reasonable oscillations and indicates that the ocean reaches some equilibrium; the data before 1950 reveal that the ocean is still in the spin-up phase of the model integration, and it is evident that the interannual anomalies have not been properly filtered out at this stage. This could explain the disagreement between the ENSO-related SSS patterns in Fig. 1b and those as extracted from in situ SSS data in Delcroix et al. (2011). So data in these years before 1950 should not be used; in the following, we will show results only during 1950–2018.

3 Signal separations and reconstructions by using the EEMD method

Multiple-scale signals coexist in the equatorial Pacific as clearly represented by ENSO and PDO phenomena. It is desirable to separate these components at different time scales. Here, such a separation is realized by using the ensemble

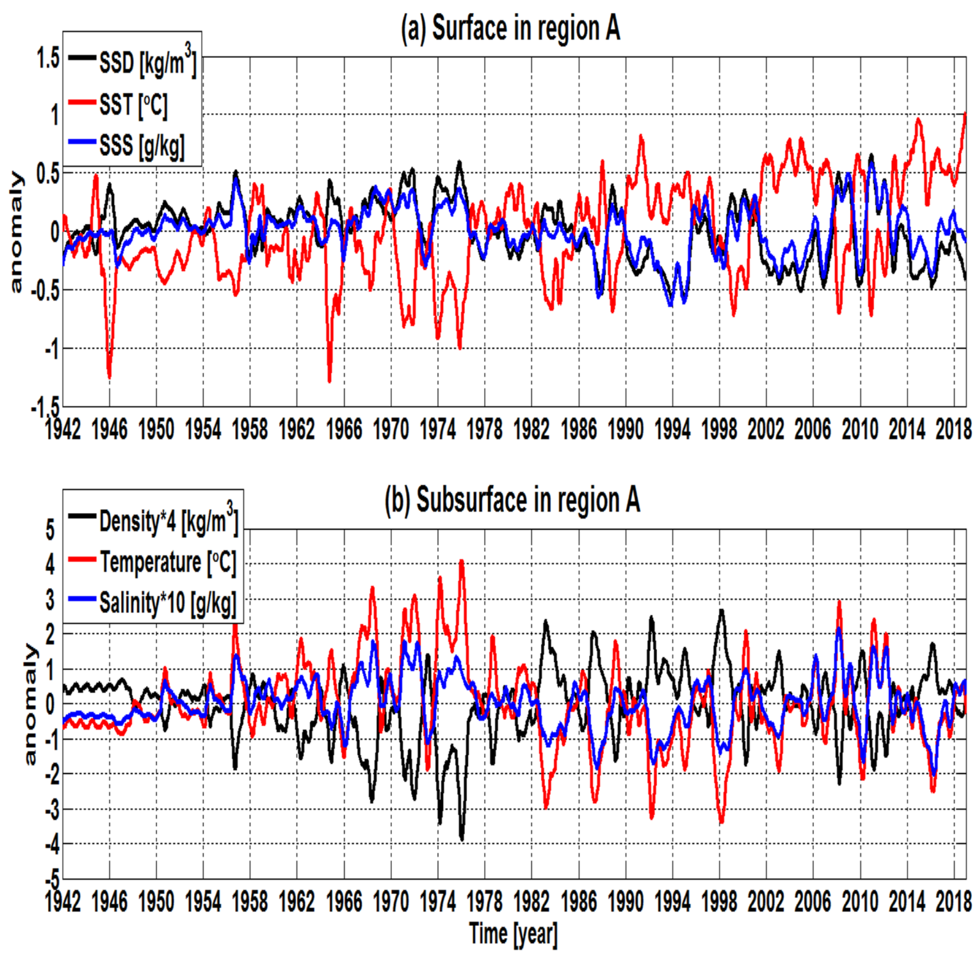

Fig. 2 Original time series of total interannual anomalies averaged in the western equatorial Pacific (the region A as indicated in Fig. 1) during the period 1942–2018: **a** SST, SSS and sea surface density (SSD); **b** temperature, salinity and density at the subsurface depth of 200 m. The salinity and density anomaly values in (**b**) are artificially multiplied respectively by 4 and 10 in the plotting for visual clarity. The units are g kg^{-1} for SSS, °C for SST, and kg m^{-3} for density

empirical mode decomposition (EEMD) method (Wu et al. 2007, 2016). The EEMD method is an enhanced EMD method by repeatedly adding the normally distributed white noise into the original signal; the resultant time series data are then subject to a regular EMD decomposition to obtain each intrinsic mode function (IMF) component. When averaging its different components, IMFn ($n = 1, 2, \ldots$), we can have each time component as the final result. Here, the white noise amplitude and the number of iterations are prescribed as 0.2 and 1000, respectively. Then, the total salinity interannual anomalies (S′) can be decomposed into a set of intrinsic mode functions (IMFs) and a long-term trend, respectively.

More specifically, the total salinity anomaly field (S′) can be decomposed into interannual, decadal, interdecadal, and trend components as follows

$$S\prime = S_{\text{interan}} + S_{deca} + S_{\text{interde}} + S_{trend},$$

in which S_{interan}, S_{deca}, S_{interde} and S_{trend} stand for interannual, decadal, interdecadal and trend components, respectively. Figure 3 illustrates examples for such a separation of the total SSS interannual variability into these temporal components. It is evident that signals are clearly separable for different time scales. For instance, the interannual component is associated with ENSO as represented by the IMF 5; the IMF 6 to IMF8 exhibit signals in the decadal and interdecadal bands. Here, we choose the IMF7 (its period is ~ 20 years) rather than IMF8 (its period is ~ 40 years) to represent the interdecadal variability because the energy of IMF7 is greater than that of IMF8. In addition, the salinity trend component shows a peak in the late 1980s, which then goes down from there, corresponding to a freshening in the 1990s and 2000s. The significance of these IMFs is tested and indicates that these extracted signals are all significant. Note that usually, low-pass filtered anomalies maybe not exploitable within a half-period at the beginning and ending of the time series. But using the EEMD method, we are confident that this is not the case as demonstrated in Wu et al. (2016).

A similar analysis is performed for temperature fields (Fig. 4), That is, the total temperature interannual anomaly field (T′) is separated into interannual, decadal, interdecadal, and trend components, respectively; well-defined variability signals and spatial patterns are seen. For example, the interannual component is associated with ENSO as represented by the IMF 5. Also, a warming trend is identified. Inspections of

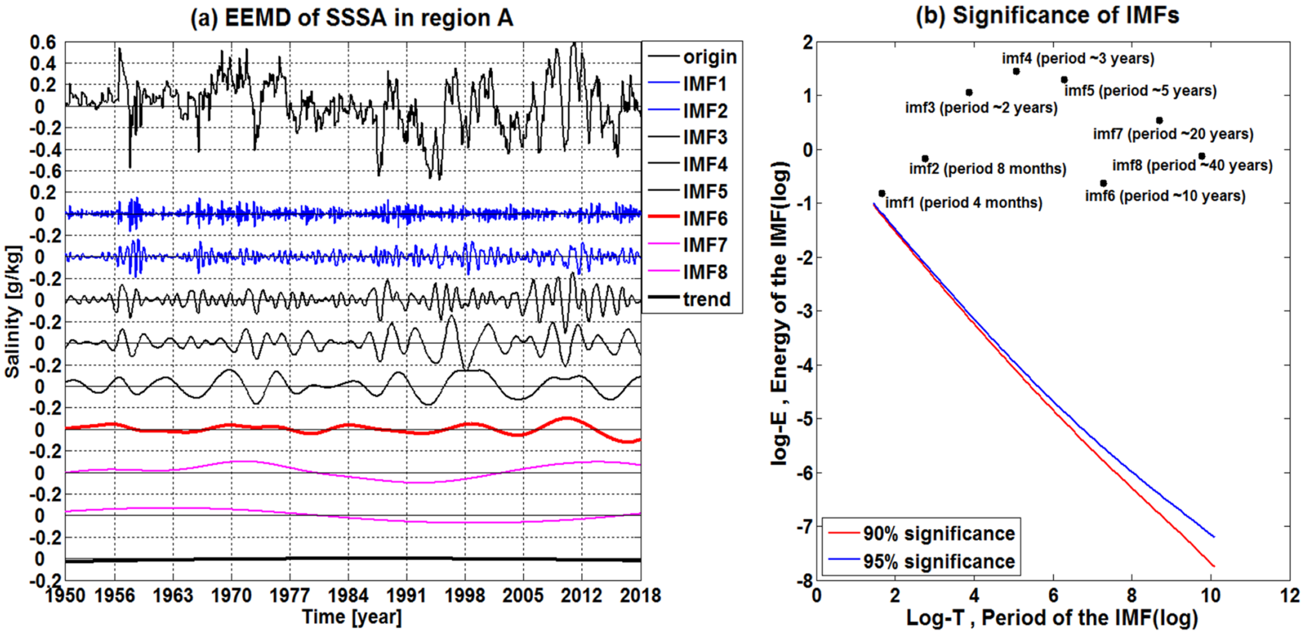

Fig. 3 Examples for the mode separations of total SSS interannual variability into temporal components at different time scales by adopting the ensemble empirical mode decomposition (EEMD) method. Shown in (**a**) are for the original time series, and respectively for a set of intrinsic mode functions (IMFs) and a long-term trend, in which the IMF 7 represents interdecadal signal, a focus in the present study. Shown in (**b**) are the tests for the significance of the IMFs

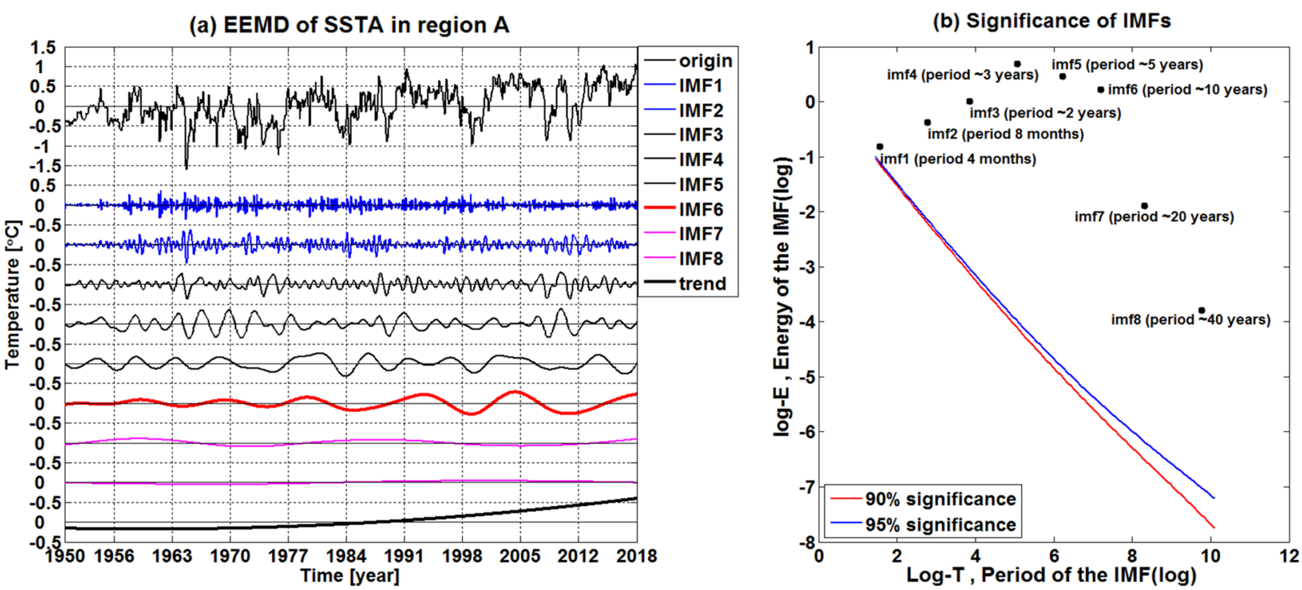

Fig. 4 The same as in Fig. 3 but for the mode separations of total SST interannual variability

these EEMD-based salinity and temperature decomposition analyses indicate their well-defined anomaly patterns and time evolutions.

Based on these signal separations, we can reconstruct a field of interest at specific frequency bands for salinity and temperature. For example, we can obtain three-dimensional anomaly fields and their evolutions for interdecadal component as follows. First, a decomposition of total interannual anomalies of salinity and temperature at each spatial grid point is performed into various temporal components: interannual, decadal and interdecadal bands, respectively. Then, salinity and temperature signal for a specific time scale can be identified from these IMFs for different temporal bands. Because the IMF7 is representing interdecadal time

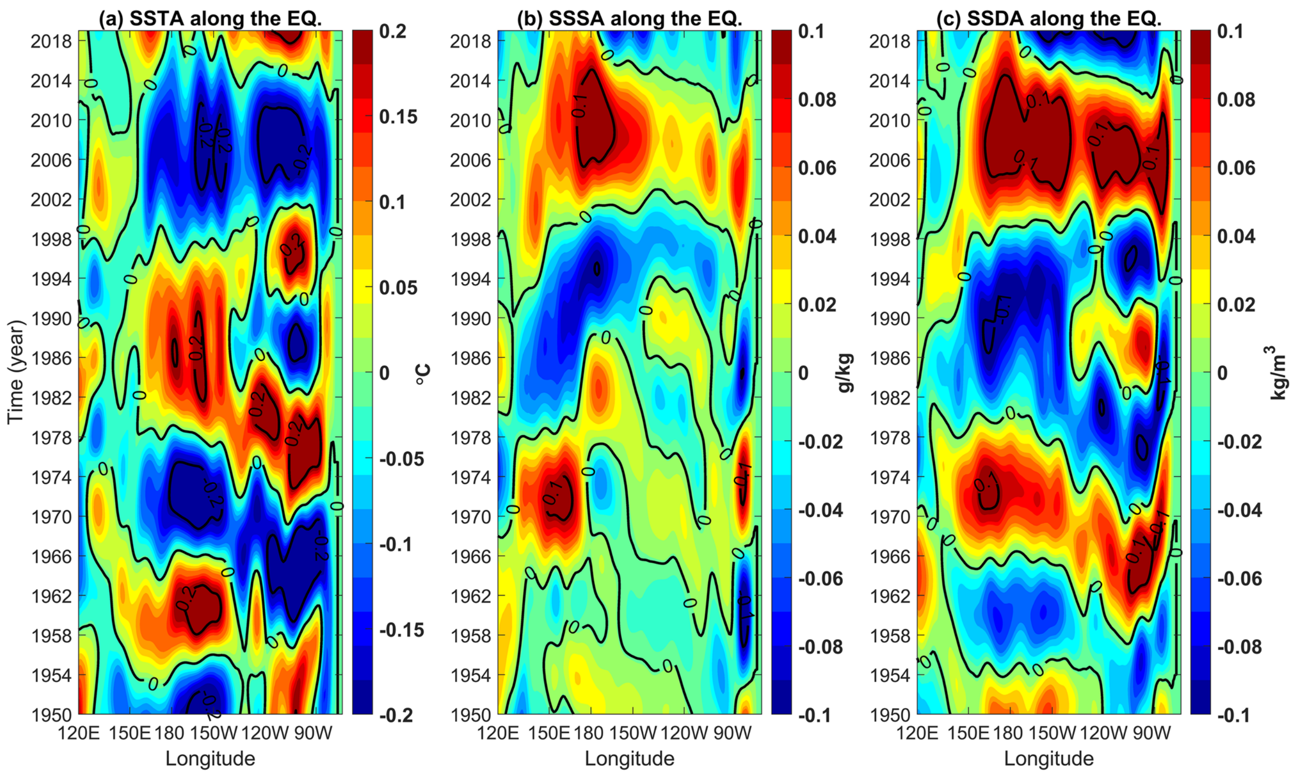

Fig. 5 Examples for the reconstructed interdecadal components for anomalies of **a** SST, **b** SSS and **c** SSD along the equator. The results are obtained using the EEMD-extracted component with signals retained to have periods around 20 years The units are °C for SST, g kg^{-1} for SSS and kg m^{-3} for SSD

scale (about 20 years), in this study, we select this component to represent interdecadal variability and then perform the corresponding reconstruction and analyses. The obtained interdecadal anomalies are relatively weak; a quantification is presented in the appendix (Fig. 19), showing the ratio of the standard deviations for SST and SSS interdecadal variabilities relative to those of total SST and SSS interannual variabilities. Quantitatively, the percentages of the interdecadal component to the total variability in the region A are 18% for SST and 20% for SSS (Fig. 18), respectively. In terms of their reconstructed interdecadal anomaly fields, then, the total T–S fields can be obtained by adding them onto the corresponding climatological fields as $S = S_{clim} + S_{interde}$ and $T = T_{clim} + T_{interde}$. In this paper, the analyses will be focused on $S_{interde}$ and $T_{interde}$ fields and their relative effects on density and other related fields.

4 The effects on density

Examples for the spatial structure and evolution of the reconstructed interdecadal variability from the IMF7 are shown in Figs. 5, 6, 7, 8 and 9. As part of climate variations, well-defined T–S anomaly relationships and their space–time evolutions are seen. The T–S relationships and their relative effects on density are examined in this section, with a focus on interdecadal signal extracted by the EEMD method ($S_{interde}$ and $T_{interde}$). The reconstructed interdecadal fields along the equator are shown in Fig. 5 for the surface layer; the vertical structures of temperature and salinity interdecadal anomalies are illustrated in Figs. 6, 7 for the western equatorial Pacific. Also, examples for their spatial patterns are shown in Figs. 8, 9, representing different phases during interdecadal evolutions.

The temperature and salinity fields exhibit pronounced interdecadal signals in the upper ocean (see Fig. 19 in the appendix, the percentage of the interdecadal component relative to the total interannual variability). For example, the interdecadal evolution can be seen to undergo persistent and transitional phases (Fig. 5). During the analysis period from 1950 to 2018, warm and fresh surface conditions persist from the late 1970s to late 1990s, and cold and salty surface conditions during the 2000s, respectively. Correspondingly, two interdecadal phase transitions are evident. One takes place around in the late 1970s from cold and salty condition to warm and fresh condition, and the other in the late 1990s from warm and fresh condition to cold and salty condition,

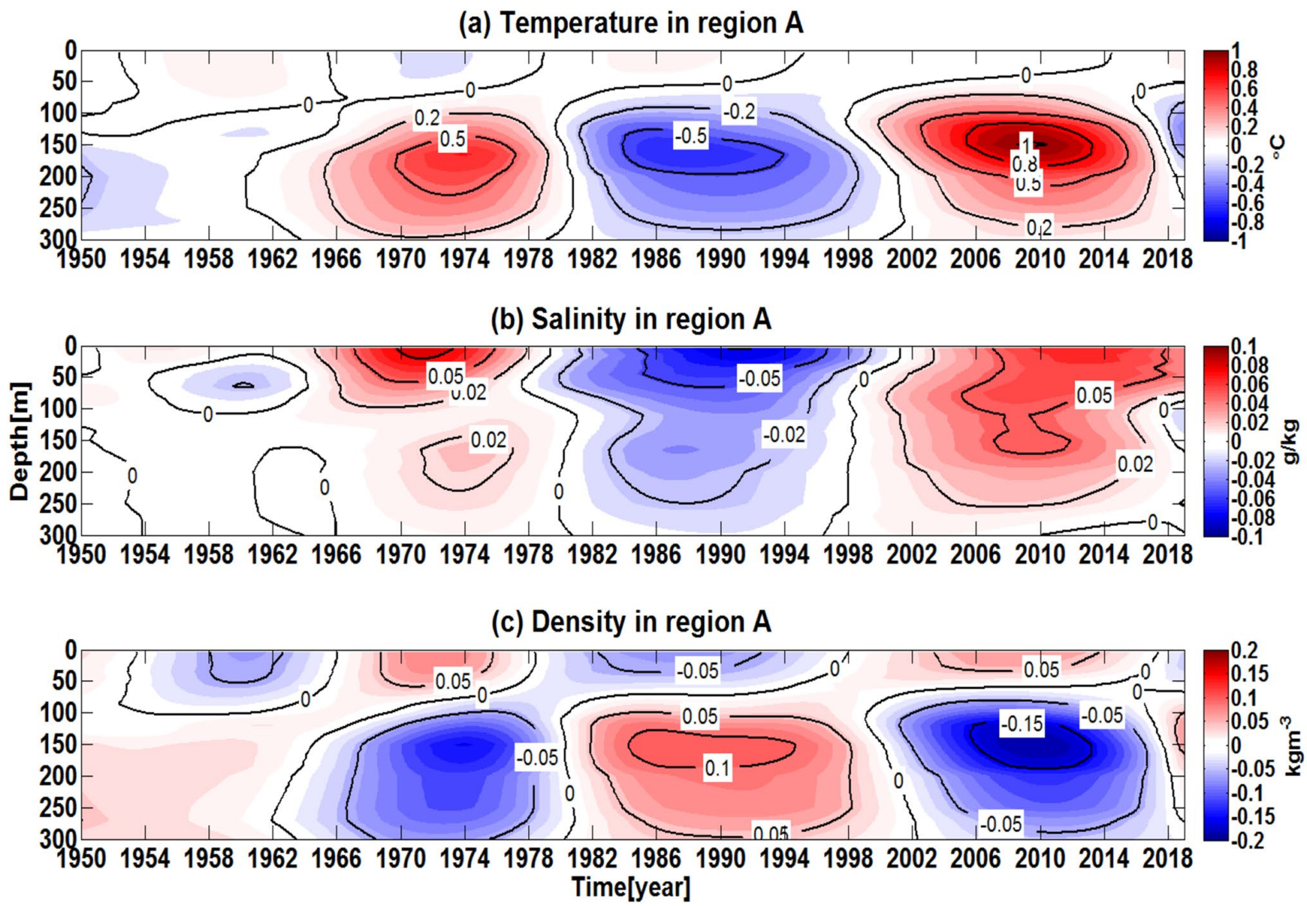

Fig. 6 The depth-time sections of the reconstructed interdecadal anomalies for temperature (**a**), salinity (**b**) and density (**c**) in the upper ocean in the region A, which is obtained using the EEMD-extracted component with signals retained to have periods around 20 years. The units are g kg^{-1} for salinity, °C for temperature, and kg m^{-3} for density

respectively. More recently, another transition is likely to take place during 2016–2018.

Vertically, a coherent T–S pattern can be seen in the upper ocean during the interdecadal evolution. Temperature anomalies are seen to have out-of-phase relationships in the surface layer and subsurface layers, with the largest anomalies occurring at the subsurface depth of 200 m (Fig. 6a). In contrast, salinity anomalies indicate a uniform sign in the upper 300 m, with the largest anomalies occurring in the surface layer (Fig. 6b). Correspondingly, salinity and temperature anomalies tend to have phase differences in the vertical during their interdecadal evolutions, being mostly out-of-phase in the surface layer but nearly in-phase in the subsurface layers (Figs. 6a, b). Case analyses for the space–time evolution characteristics and salinity effects are detailed below.

4.1 The persistent phases

As mentioned above, temperature anomalies exhibit out-of-phase signs in the surface layer and in the subsurface layers (Figs. 6a and 7), whereas salinity anomalies have the nearly in-phase sign in the upper ocean (Fig. 6b). Their corresponding combined effects on density exhibit clear differences in the upper ocean during interdecadal evolution (Figs. 6c and 7).

(1) In the surface layer

Figure 8 shows the reconstructed SSS and SST interdecadal anomaly fields in the tropical Pacific for the persistent phases, as represented during the 1980s and 1990s for warm and fresh conditions, and during the 2000s for cold and salty conditions, respectively. Spatially, large SSS anomalies are located in the western Pacific, which mainly reflects the zonal migration of the fresh pool along the equator. A pronounced covarying pattern in salinity and temperature is seen in the western equatorial Pacific. In the surface layer, SSS and SST anomalies tend to be of the opposite sign during the persistent phases, with their effects being density-uncompensated. For example, positive SST anomalies are accompanied by negative SSS anomalies during the 1980s–1990s (the left panels in Fig. 8); these individual anomalies both contribute to negative density anomalies. So, their combined effects lead

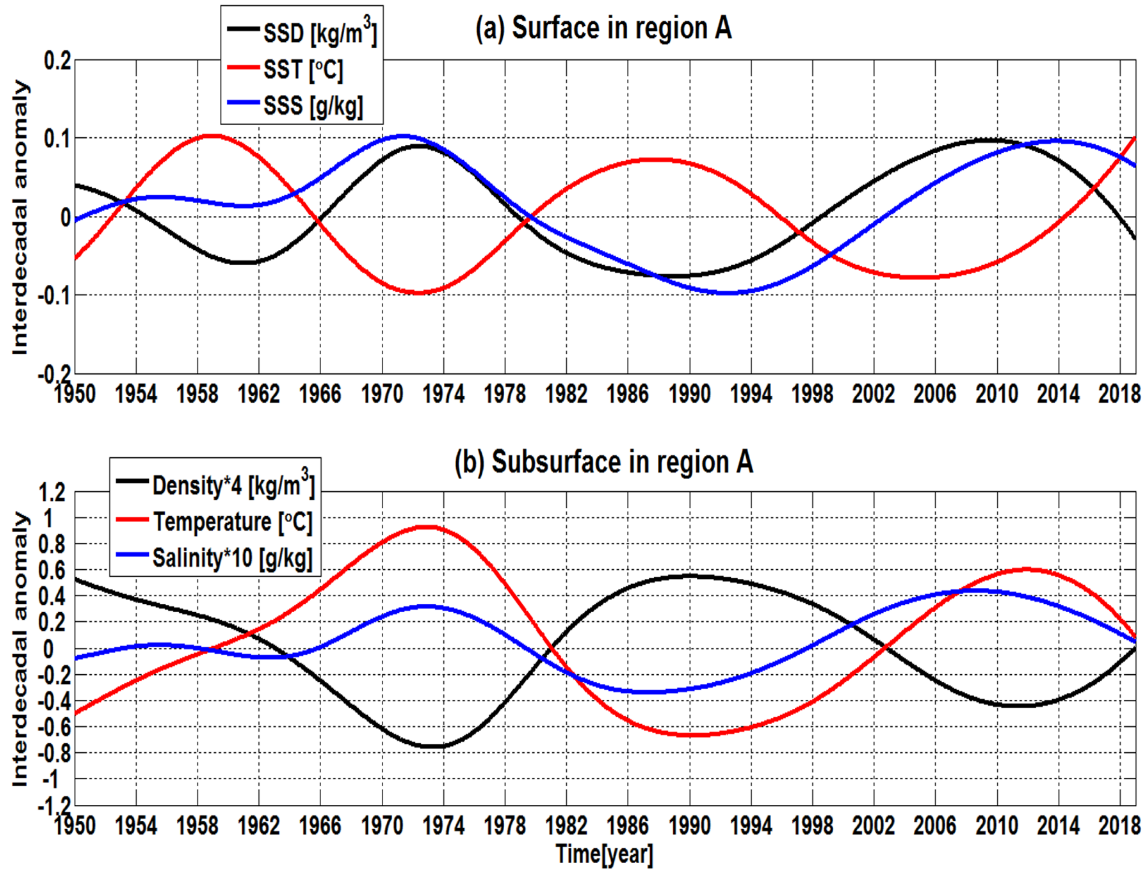

Fig. 7 The time series of the reconstructed interdecadal anomalies for salinity, temperature and density at the sea surface (**a**) and at subsurface depth of 200 m (**b**) in the region; the results are obtained using the EEMD-extracted component with signals retained to have periods around 20 years. The salinity and density anomaly values in (**b**) are artificially multiplied respectively by 4 and 10 in the plotting for visual clarity. The units are g kg^{-1} for salinity, °C for temperature, and kg m^{-3} for density

to the negative density anomalies that become more negative as compared with those induced by temperature or salinity alone. During cold and salty phase in the 2000s (the right panels in Fig. 8), an opposite situation takes place. Cold SST anomalies produce positive density anomalies; the effects of negative salinity anomalies make the temperature-produced positive density anomalies more positive. So, the amplitude of density variability is enhanced due to the uncompensated salinity effects.

Because the effect of salinity anomalies on density in the surface layer is comparable to that of temperature anomalies, salinity is expected to make an important contribution to density variability. As shown in Fig. 7a, for example, the phase transitions of SSD interdecadal anomalies do not immediately follow SST, with a delay of the former relative to the latter; this delay is caused by SSS effect. A lagged correlation analysis among interdecadal anomalies of SSD, SST and SSS is presented in the appendix (Fig. 20). For example, it is evident that the phase transitions of SSD interdecadal anomalies lead SSS, as indicated by the maximum correlation coefficient between SSD and SSS anomalies which is reached (0.8) when the SSS is lagging the SSD by 2 years. So, the phase transitions of SSD anomalies are delayed relative to SST anomalies due to SSS effects; otherwise, the former would follow those of SST anomalies. The relative contributions of individual salinity and temperature anomalies to density and other related fields will be quantified in Sect. 5.

(2) In the subsurface layers

In the western equatorial Pacific, large temperature anomalies are seen in the subsurface layers, whereas large salinity anomalies are located in the surface layer. In addition, subsurface salinity anomalies tend to have the same sign with those of temperature during interdecadal evolution (Figs. 6, 7); so, salinity anomalies present a compensated effect on density, relative to temperature in the subsurface layers. During the 1980s–1990s, for example, negative temperature anomalies are accompanied by negative salinity anomalies: the former gives rise to positive density anomalies but the latter contributes to negative density anomalies, respectively. Their combined effects lead to the positive

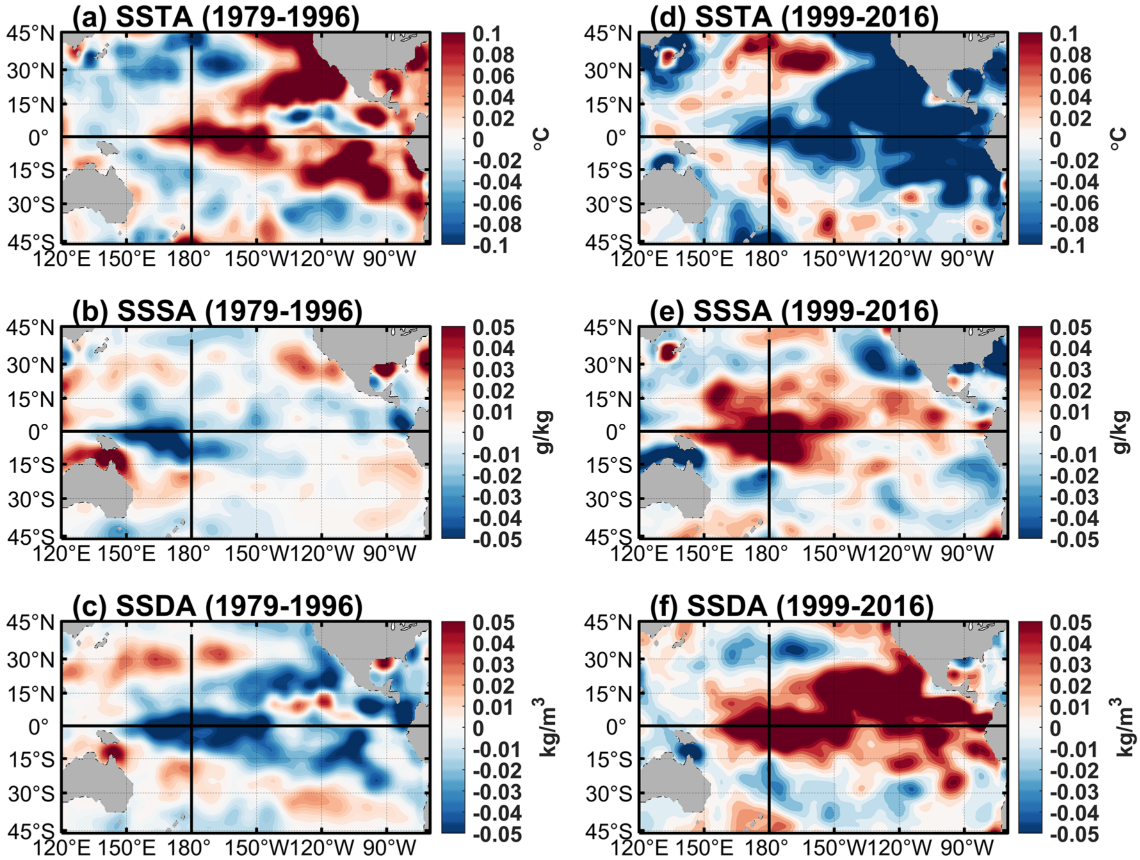

Fig. 8 Examples for horizontal distributions of the reconstructed interdecadal components for anomalies of **a**, **d** SST, **b**, **e** SSS and **c**, **f** SSD in the tropical Pacific during 1979–1996 (the left panels) and during 1999–2016 (the right panels), respectively; these periods represent persistent interdecadal phases. The units are °C for SST, g kg^{-1} for SSS and kg m^{-3} for SSD

density anomalies that become reduced (compensated) as compared with those produced by temperature alone. Nevertheless, interdecadal variability of salinity is weak in the subsurface layer relative to that of temperature; so salinity effect on density is weak. Thus, density interdecadal anomalies are dominantly determined by temperature. During the 2000s, the relationships among these anomalies and salinity effects are in an opposite sense (Figs. 8, 9). Because the effects of temperature are greater than those of salinity, density anomalies are of the opposite sign with temperature.

(3) Differentiated salinity effects on vertical stratification in the upper ocean

During the interdecadal persistent phases, salinity and temperature anomalies tend to be largely of the opposite sign in the surface layer (Fig. 7a), but to be nearly of the same sign in the subsurface layers (Fig. 7b). Correspondingly, salinity has density-uncompensated effect in the surface layer, giving rise to enhanced SSD anomalies. In contrast, salinity has density-compensated effect in the interior subsurface layers, producing density anomalies that are reduced. As such, salinity anomalies tend to have asymmetric effects on density in the surface layer and subsurface layer, respectively.

Such a differentiated salinity effect on density in the vertical direction acts to produce large density gradient, and so the vertical stratifications should be more strongly affected (see Sect. 5 for more details), which can further modulate vertical mixing and SST. For example, during warm and fresh interdecadal persistent periods in the 1980s-1990s (Figs. 5a, b and 6), warm SST anomalies and negative SSS anomalies (being of the opposite sign) have uncompensated effects on density, in which the latter makes the negative density anomalies more negative in the surface layer. But in the subsurface layers (Fig. 6), the negative temperature and salinity anomalies (being of the same sign) have compensated effects, with the salinity effect making the positive density anomalies less positive. So, salinity effects give rise to an increased contrast of density in the upper ocean and thus produces more stable vertical stratification, which acts to suppress the vertical mixing and sustain the warm SST anomalies. This indicates an enhancing effect on SST. During cold and salty interdecadal persistent phases in the 2000s, the relationships among these anomaly fields

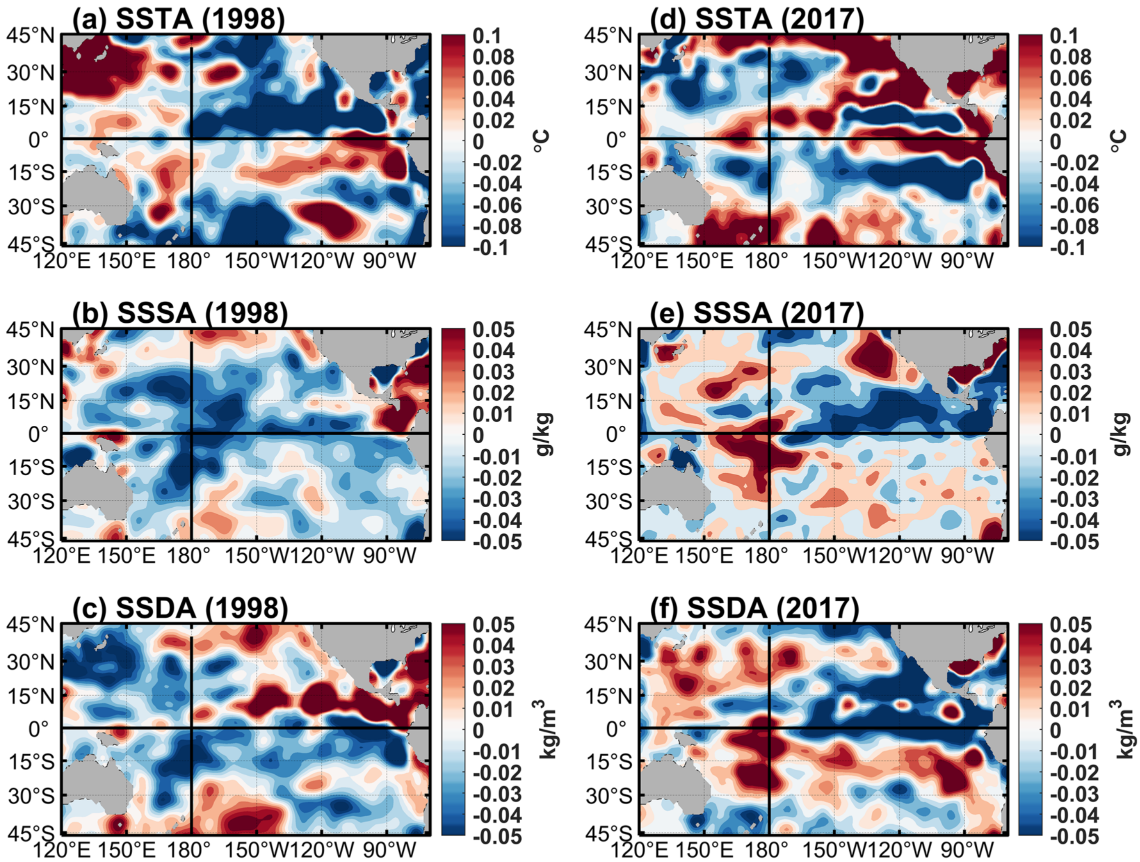

Fig. 9 Examples for horizontal distributions of the reconstructed interdecadal components for anomalies of **a**, **d** SST, **b**, **e** SSS and **c**, **f** SSD in the tropical Pacific during the transitional period as represented in 1998 (the left panels) and in 2017 (the right panels). The units are °C for SST, g kg^{-1} for SSS and kg m^{-3} for SSD

and salinity effects are in an opposite situation, in which positive salinity anomalies in the upper ocean cause more positive density anomalies in the surface layer, but less negative density anomalies in the subsurface layers. So, the salinity effects cause weaker gradient of density in the upper ocean and less stable stratification, helping sustain the cold SST anomalies. Thus, salinity-induced effects act to enhance local SST anomalies during interdecadal persistent phases.

4.2 The transitional periods

The interdecadal persistent conditions are seen to transit into their opposite condition in relatively short periods (Fig. 5). The corresponding vertical structures are demonstrated in Figs. 6, 7. Examples for horizontal distributions of the reconstructed interdecadal anomalies for SSS, SST and SSD are shown in Fig. 9 for transitional periods as represented in years 1998 and 2017, respectively. Here, we define the transitional periods during which SSD anomalies change signs; due to the differences in sign changes, transitional periods can differ when using different fields of SST, SSS and SSD anomalies. During the transitional periods, temperature and salinity anomalies exhibit clear differences in their sign changes in the vertical direction between the surface layer and subsurface layers: temperature anomalies undergo out-of-phase transitions in the surface layer and in the subsurface layers (Fig. 6a), whereas salinity anomalies have the nearly in-phase sign changes in the upper ocean (Fig. 6b). Vertically, as represented in 1998 and 2017, temperature and salinity anomalies exhibit clear differences in their sign transitions in the surface layer, but largely in-phase sign transitions in the subsurface layer. In this subsection, such situations are further analyzed in more detail, with case analyses being highlighted for the interdecadal transitions occurring in the late 1990s and early 2000s.

(1) The surface layer

Although SST and SSS anomalies in the western equatorial Pacific are largely of the opposite sign during the persistent phases (Fig. 7), they can be of the same sign during the transitional periods. One striking case can be noted from these anomaly relationships during transitional periods in

1995–2002 (Fig. 7), when SSS anomalies exhibit the same sign with SST anomalies. In such a case, salinity is seen to have the compensated effects on density. As the effect of salinity variability on density in the surface layer can be comparable to that of temperature, salinity can play an important role in determining density anomalies during the transitional periods.

More detailed evolutions can be analyzed as follows. During the interdecadal persistent phases in the 1980s-1990s, warm SST anomalies and negative SSS anomalies are seen in the western equatorial Pacific; their effects are density-uncompensated, leading to enhanced density anomalies. Then, a phase transition occurs in the late 1990s through early 2000s (Fig. 7a). A striking feature here is that temperature and salinity anomalies during 1995–2002 are of the same signs, with their effects being thus density-compensated. Among anomalies of SST, SSS and SSD, SST is seen to take a transition firstly in 1995 and becomes cold anomaly (contributing to a positive density anomaly); at this time, SSS anomalies remain negative until 2002 (contributing to negative density anomaly). Note that the corresponding density anomalies remain to be negative until around 1999 and then become positive. Thus, the sign of density anomalies during 1995–1999 does not follow the change in temperature (which becomes negative in 1995). Clearly, the phase transition of the negative density anomaly is delayed relative to temperature due to the effect of the negative salinity anomalies. This means that the contribution of negative salinity anomalies to the negative density anomalies during 1995–1998 is even greater than that of the negative temperature anomalies; so, the sign of negative density anomalies is determined dominantly by negative salinity anomalies.

Another case is also seen for the dominant salinity effects on sign transitions of density anomalies during 2014–2018, when positive SST anomalies are accompanied by positive SSS anomalies. Because these anomalies are of the same sign, their effects are density-compensated. The fact that the corresponding density anomalies remain positive until 2018 indicates that the positive SSS anomalies play a dominant role in determining the sign of the positive density anomalies. Detailed inspections further indicate that there is a delay in phase transition of the positive density anomaly in 2018 due to the positive salinity anomaly effect; without the salinity effect, otherwise, density would transit into its negative anomalies earlier in 2014 as SST transits into positive anomalies. This means that the effect of positive salinity anomalies on density is even greater than that of positive temperature anomalies so that the sign of positive density anomalies is determined dominantly by positive salinity anomaly contribution.

(2) The subsurface layers

Clear transitions are also seen in the subsurface layers during interdecadal transitional periods (Fig. 7b); salinity and temperature anomalies are nearly of the same sign, with little phase differences in their sign changes. So, salinity is seen to have a compensating effect on density relative to temperature. Because the effect of salinity variability is smaller compared with that of temperature, salinity-induced compensated effects are weak. Density anomalies are dominantly determined by temperature. Indeed, the sign of density anomaly follows closely that of temperature during interdecadal transitional periods. In addition, the phase transitions in the subsurface layers (Fig. 7b) and surface layer (Fig. 7a) indicate different lag-lead relationships. For example, if we use SSD changes in sign as an indicator of phase transition, the subsurface transition lags the surface transition by ~ 2 years around 1980, ~ 4 years around 2000, ~ 1 year around 2018, but leads it by ~ 3 years around 1965, respectively.

(3) The compensated salinity contribution to density and enhancing effects on SST

During the transitional periods as represented in 1998 and 2017 (Fig. 9; Figs. 7, 8), the sign transitions for anomalies of SST, SSS and SSD exhibit clear differences in the western equatorial Pacific, indicating the differences in the T–S relationships and salinity-induced effects on SST. One notable feature is that salinity effects indicate an obvious shift from being density-uncompensated during the persistent phases to being density-compensated during the transitional periods, respectively. During the transitional period, for example, SST and SSS anomalies can be of the same sign, with their SSD-compensated effects, and then the sign of density anomalies can be even determined by salinity anomalies. As specifically represented in 1998 (Fig. 9), negative SST anomalies are accompanied by negative SSS anomalies (Fig. 7a); the former causes an increase in density, but the latter gives rise to a decrease in density. Thus, salinity has density-compensated effects, acting to maintain negative density anomalies in the surface layer during this transitional period (being lighter); this causes more stable stratification in the upper ocean, which leads to a decrease in vertical mixing, having a weakening effect on the cold SST anomalies. So, SSS-induced effect in the surface layer indicates a suppressing effect on the cold SST anomalies during the transitional periods. This situation is very different from that during the persistent phases, when SSS effects act to enhance warm SST anomalies.

5 The relative contributions of salinity and temperature anomalies

Large salinity interdecadal variability in the western equatorial Pacific is seen to play an important role in contributing to density anomalies. The relative contributions of temperature and salinity anomalies to density can be further quantified by separating their individual effects. In this section, we present some related analyses.

The reconstructed interdecadal components of temperature and salinity anomalies can be added onto their climatological parts to form total fields: $S = S_{clim} + S_{interde}$, $T = T_{clim} + T_{interde}$. A diagnostic analysis is then performed to quantify their individual contributions to a field of interest (F); its interdecadal anomalies can be calculated by considering temperature and salinity to be interdecadally varying ($T_{interde}$ and $S_{interde}$) or climatological (T_{clim} and S_{clim}), respectively. $F(T_{interde}, S_{interde})$ denotes a reference analysis in which both temperature and salinity fields are taken to be interdecadally varying in calculating F; $F(T_{interde}, S_{clim})$ is for a thermosteric analysis in which temperature field is taken as interdecadally varying but salinity field is kept as climatological; $F(T_{clim}, S_{interde})$ is for a halosteric analysis in which salinity is taken as interdecadally varying but temperature field is kept to be climatological; $F(T_{clim}, S_{clim})$ is a climatological field in which temperature and salinity fields are both kept as climatological in calculating F, serving as a climatology from which interdecadal anomalies are calculated. As demonstrated above, density anomalies in the western region can be equally importantly contributed from salinity. So, a focused analysis is placed on the western equatorial Pacific in the region A (6°S–4°N, 150°E–180°). Detailed attribution analyses are given below for relative contributions of temperature and salinity anomalies to interdecadal anomalies of density and N^2, respectively.

(1) Density (ρ)

Figure 10 displays the results from diagnostic calculations performed to quantify the relative contributions of $T_{interde}$ and $S_{interde}$ to density anomalies in the upper ocean of the western equatorial Pacific (the region A); the corresponding time series are shown in Fig. 11 for the sea surface and at subsurface depth of 200 m, respectively. As evident, $\rho(T_{interde}, S_{interde})$ is nearly the sum of $\rho(T_{interde}, S_{clim})$ and $\rho(T_{clim}, S_{interde})$. Detailed inspection of these anomaly fields indicates that the way density is affected in the upper ocean is varying during the interdecadal evolution. In the subsurface layers, the situation is quite simple (Fig. 11b), in which salinity and temperature anomalies are largely of the same sign, with density anomalies being dominantly attributed from temperature. Indeed, $\rho(T_{interde}, S_{interde})$ follows closely $\rho(T_{interde}, S_{clim})$ in the subsurface layer (Fig. 11b).

The situation is more complicated in the surface layer (Fig. 11a), which will be our focus in the following analyses. As demonstrated above, salinity in the surface layer can have both uncompensated and compensated effects on density. During the persistent phases, SSS and SST anomalies are largely of the opposite sign; thus, their contributions to density anomalies are in the same direction, acting to increase density anomalies. The relative effects of $T_{interde}$ and $S_{interde}$ on density are well reflected in these three calculations for density anomalies (Figs. 10 and 11a). During the persistent phases, for example, SSS and SST anomalies are of the opposite sign and the corresponding $\rho(T_{interde}, S_{clim})$ and $\rho(T_{clim}, S_{interde})$ fields are not compensated, making the amplitude of $\rho(T_{interde}, S_{interde})$ larger. During the transitional periods, on the other hand, SSS and SST anomalies can be of the same sign and their effects are thus density-compensated. So, the $\rho(T_{interde}, S_{clim})$ and $\rho(T_{clim}, S_{interde})$ fields make the amplitude of $\rho(T_{interde}, S_{interde})$ smaller, consistent with the analyses in the Sect. 4. One striking feature is that the sign and amplitude of $\rho(T_{interde}, S_{interde})$ can be determined by $\rho(T_{clim}, S_{interde})$ due to the dominant effect of salinity.

One interesting case can be illustrated in more details during the transitional periods as indicated during 1995–2003, when anomalies of SST, SSS and SSD indicate obvious differences in their sign transitions (Fig. 7). As analyzed above, for example, negative SST anomalies are accompanied by negative SSS anomalies, acting to produce more negative density anomalies during 1995–1999 (Fig. 7a). The delayed effects on sign transitions of the negative density anomalies are well reflected in these three density calculations (Fig. 11a). For example, $\rho(T_{interde}, S_{clim})$ takes a lead in transition into positive anomaly firstly in 1995; $\rho(T_{clim}, S_{interde})$ takes a late transition into positive anomaly in 2002 (a lag); $\rho(T_{interde}, S_{interde})$ remains to be negative anomaly until 1999 and then transits into its positive anomaly; so, there is a lag caused by salinity effects relative to $\rho(T_{interde}, S_{clim})$. The comparisons among these three density calculations indicate that negative salinity anomaly is making a dominant contribution to the negative SSD anomaly (Fig. 11a).

Quantitatively, Fig. 12 presents the relative contributions of salinity and temperature anomalies to density and the other related fields during different phases of the interdecadal evolution. These calculations indicate that salinity can play a dominant role in producing density anomalies during interdecadal transitional periods. For example, the negative SSD anomaly in 1998 ($-$ 0.003 kg m^{-3}) is attributed to the combined effects of a negative SSS anomaly ($-$ 0.044 kg m^{-3}) and a negative temperature anomaly (+0.041 kg m^{-3}), respectively. Also for the transitional period in 2017, the positive SSD anomaly in 2017 (+0.01 kg m^{-3}) is attributed to the combined effects of a positive SSS anomaly (+0.064 kg m^{-3}) and a positive temperature anomaly (-0.054 kg m^{-3}), respectively. Clearly, salinity anomalies play an important role in determining not only the amplitude but also the sign of density anomalies during the interdecadal evolution.

(2) The Brunt–Väisälä frequency squared (N^2)

Density interdecadal anomalies are used to calculate its vertical gradient and the corresponding Brunt–Väisälä

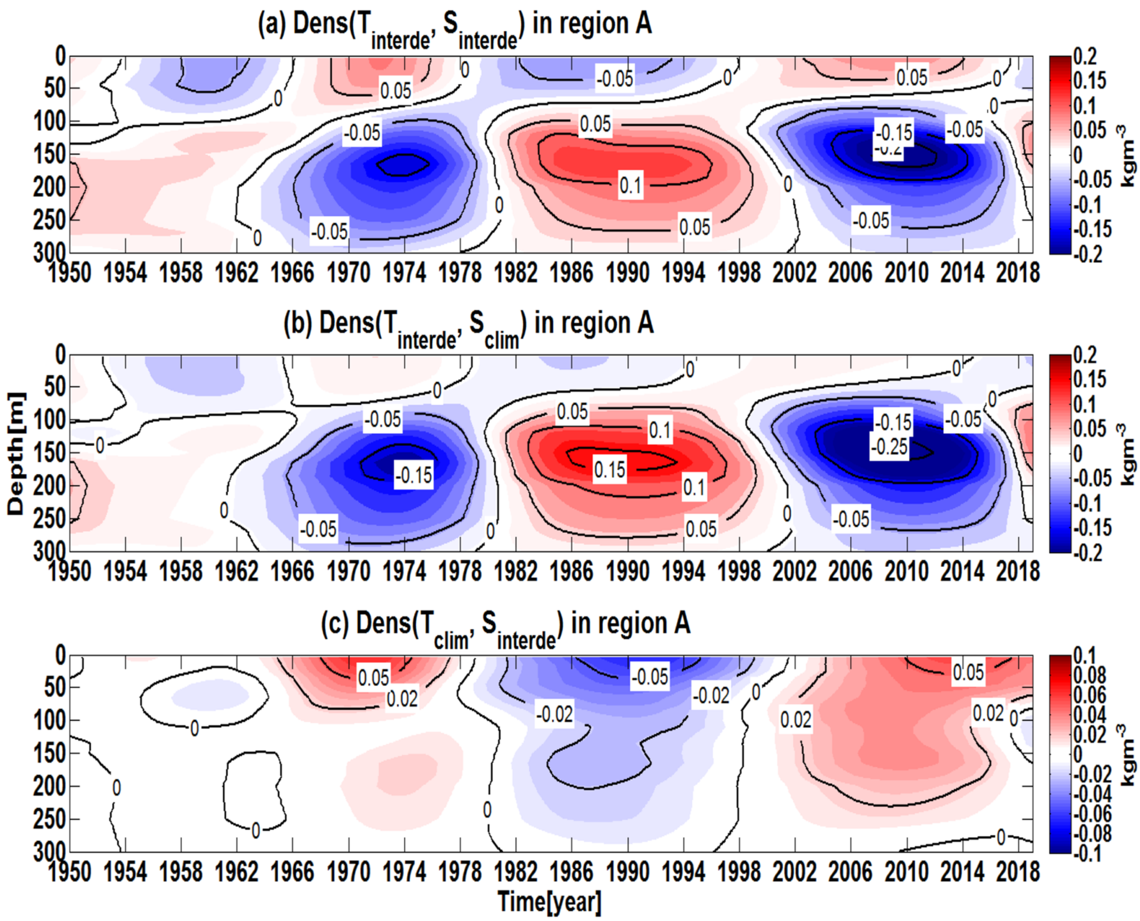

Fig. 10 Results from diagnostic calculations performed to quantify the relative contributions of interdecadal components ($T_{interde}$ and $S_{interde}$) to density anomalies in the region A. Shown are the depth-time sections of density anomaly fields for **a** $\rho(T_{interde}, S_{interde})$, **b** $\rho(T_{clim}, S_{interde})$, and **c** $\rho(T_{interde}, S_{clim})$. These density anomalies are calculated relative to its climatological density field (i.e., $\rho(T_{clim}, S_{clim})$). Note different color bar and contour are used in (**c**). The unit is kg m^{-3} for density

frequency squared (N^2), a parameter representing the stratification stability. The vertical structure of interdecadal variability for N^2 in the upper ocean of the western equatorial Pacific is shown in Fig. 13, which corresponds well to that for density (Fig. 6c). On interdecadal time scales, N^2 anomalies exhibit well-defined see-saw patterns vertically with large anomalies centered at depths of 100 m and 200 m, respectively. During the interdecadal evolution, transitions take place between more stable and more unstable stratification conditions in the upper ocean. For example, during warm and fresh phases in the 1980s-1990s, the stratification is more stable in the upper 150 m, but less stable below it. A transition takes place during transitional period in the late 1970s and late 1990s, respectively. During the cold and salty phases in the 2000s, then, the stratification becomes less stable in the upper layer of 150 m but more stable below it. Such changes can be explained by changes in density, which are attributed to temperature and salinity effects. In the subsurface layers, as demonstrated above, salinity and temperature anomalies are of the same sign during the interdecadal evolution and their effects are density-compensated; so, N^2 anomalies are dominantly determined by changes in the vertical structure of temperature.

The situation is quite complicated in the surface layer, where salinity can have both uncompensated and compensated effects on density during interdecadal evolution. As seen above, salinity anomalies exhibit the differences in its effects on density in the upper ocean: an enhancing density-uncompensated effect in the surface layer, but a reducing density-compensated effect in the subsurface layers, respectively. These salinity effects on density are well reflected in its vertical gradient (N^2). For example, during warm and fresh persistent phases, the negative SSS anomalies make the SST-induced negative SSD anomalies *more negative*, thus making more stable stratification in the upper layer of 150 m. Similarly, during cold and salty persistent phases, positive SSS anomalies make the SST-induced positive SSD anomalies *more positive*, thus making less stable stratification in the upper layer. During the transitional periods, the sign and

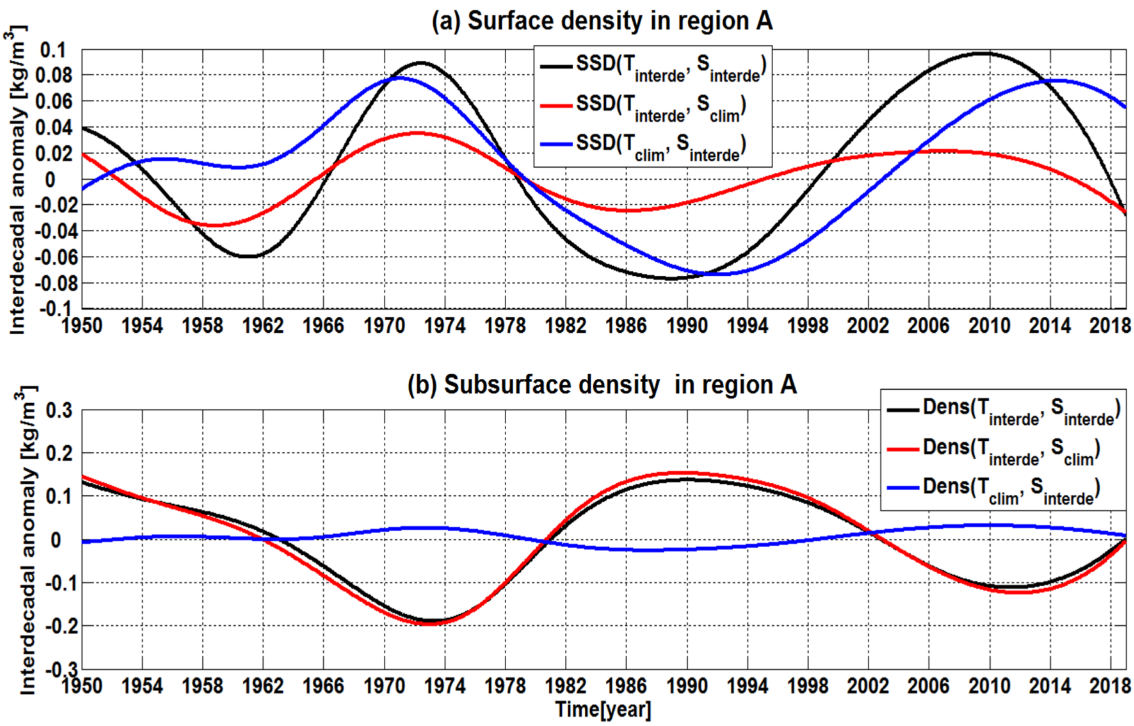

Fig. 11 The same as in Fig. 10 but for the corresponding time series of the three calculated density anomaly fields at the sea surface (**a**) and at subsurface depth of 200 m (**b**). The unit is kg m^{-3} for density

amplitude of SSD anomalies can be dominantly determined by salinity, and so of N^2 anomalies.

Similar attribution analyses are performed for the effects of $T_{interde}$ and $S_{interde}$ on N^2 interdecadal anomalies. The extent to which N^2 is affected by salinity is shown in Fig. 13 for three diagnostic calculations to quantify the relative contributions of $T_{interde}$ and $S_{interde}$ in the western equatorial Pacific; the corresponding time series are shown in Fig. 14 for the sea surface and at subsurface depth of 200 m, respectively. As evident, the sum of $N^2(T_{interde}, S_{clim})$ and $N^2(T_{clim}, S_{interde})$ almost recovers the signal of $N^2(T_{interde}, S_{interde})$. In the subsurface layers (Fig. 14b), $N^2(T_{interde}, S_{interde})$ is dominantly determined by temperature in the western equatorial Pacific so $N^2(T_{interde}, S_{interde})$ follows closely $N^2(T_{interde}, S_{clim})$. As shown in Fig. 14a, the salinity effects on N^2 are mainly in the surface layer, where salinity plays a dominant role in producing N^2 anomalies during the transitional period, with $N^2(T_{interde}, S_{interde})$ closely following $N^2(T_{clim}, S_{interde})$. These analyses indicate that salinity effect in the surface layer can make dominant contribution to the stratification change, including the amplitude and sign of N^2 variability during the transitional period.

Quantitatively, Fig. 12 shows the relative contributions of salinity and temperature anomalies to N^2 in the western equatorial Pacific during different periods. These calculations indicate that salinity can play an important role in producing N^2 anomalies during interdecadal evolution. For example, the positive N^2 anomaly ($+1.078\times10^{-5}$ s^{-2}) for the transitional period in 1998 is attributed to the combined effects of a negative SSS anomaly ($+0.685\times10^{-5}$ s^{-2}) and a negative temperature anomaly ($+0.392\times10^{-5}$ s^{-2}), respectively. Also for the transitional period in 2017, the negative N^2 anomaly in 2017 (-0.712×10^{-5} s^{-2}) is attributed to the combined effects of a positive SSS anomaly (-0.641×10^{-5} s^{-2}) and a positive temperature anomaly (-0.072×10^{-5} s^{-2}), respectively. Clearly, salinity anomalies play an important role in determining not only the amplitude but also the sign of N^2 anomalies during the transitional phase.

6 Conclusion and discussion

Ocean salinity and temperature anomalies exhibit multiple-scale variability signals in the tropical Pacific. Their reanalysis data are used to derive interannual anomalies relative to seasonally varying climatology, which are then subject to the EEMD into separable signals for interannual, decadal, interdecadal bands, and a trend component, respectively. Large salinity interdecadal variability is seen in the upper ocean over the western equatorial Pacific. Because the effect of salinity interdecadal variability on density is comparable to that of temperature in the region, salinity can play an important role in contributing to density anomalies. A focus of this study is

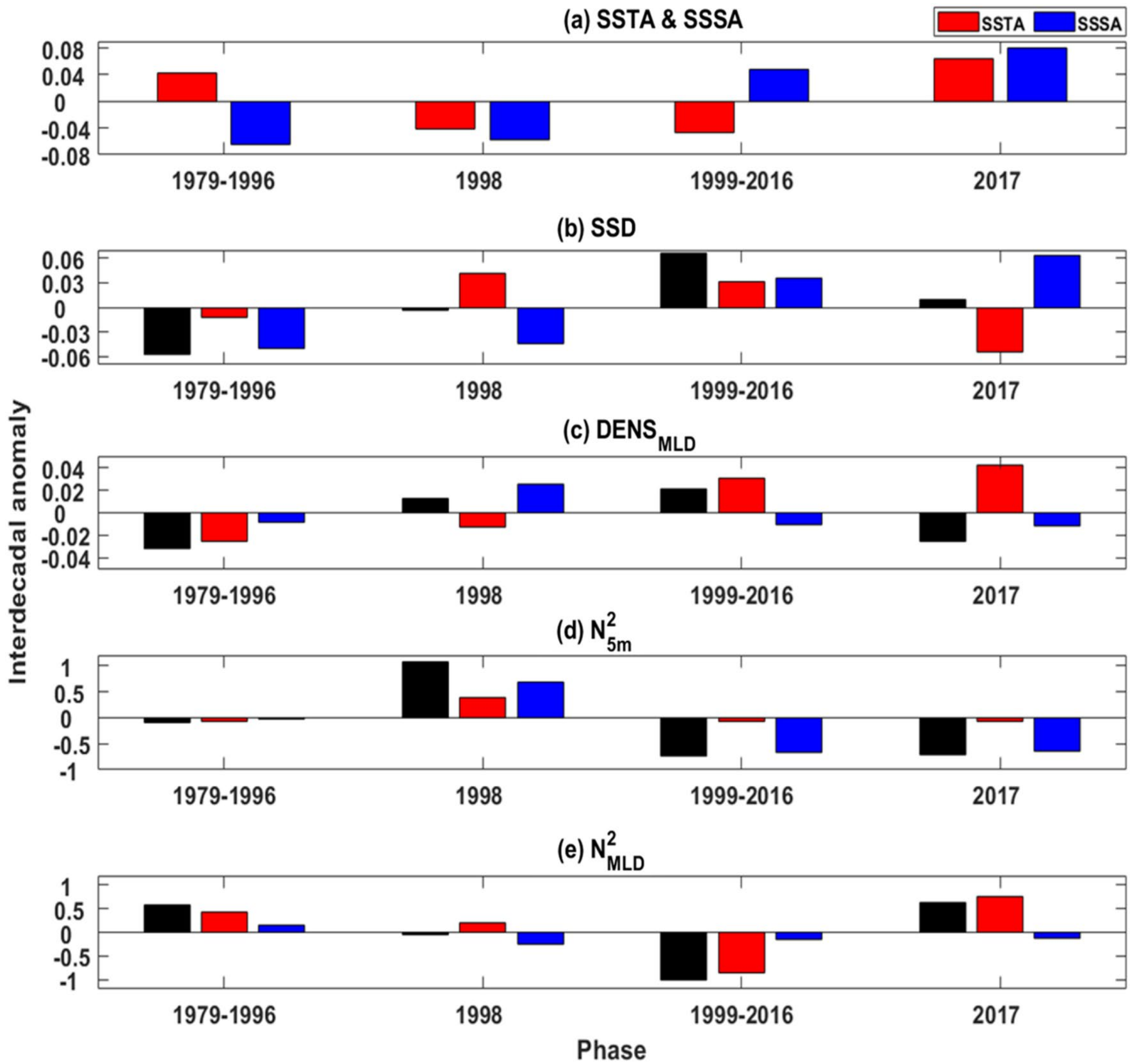

Fig. 12 Interdecadal anomalies of temperature, salinity and some derived fields, which are calculated in the western equatorial Pacific (the region A) during different periods representing interdecadal evolution; the resultant fields include SST, SSS, sea surface density (SSD), the mixed layer (ML) depth (MLD), oceanic density at the base of ML ($DENS_{MLD}$), N^2 near the sea surface at 5 m (N^2_{5m}) and at the base of ML (N^2_{MLD}), respectively. **a** SSTA (red box) and SSSA (blue box); **b** SSD for the three calculations performed to quantify individual contributions of temperature and salinity fields (see the text for detail), using both interdecadal temperature and salinity fields (black box), interdecadal temperature and climatological salinity fields (red box), and climatological temperature and interdecadal salinity fields (blue box), respectively; **c** $DENS_{MLD}$ for the three calculations [the same way as in (**b**)]; **d** N^2_{5m} for the three calculations [the same way as in (**b**)]; **e** N^2_{MLD} for the three calculations [the same way as in (**b**)]. Results are shown for the persistent phases in 1979–1996 and 1999–2016, and for the transitional periods as represented in 1998 and 2017, respectively

on salinity interdecadal variability and its effect on density and stratification in the western equatorial Pacific. A diagnostic calculation is performed to quantify the relative contributions of temperature and salinity anomalies to variabilities of density and the related stratification in the region.

Salinity interdecadal variability indicates a uniform anomaly pattern with the same sign in the upper ocean of 200 m, whereas temperature variability exhibits out-of-phase anomaly patterns in the surface layer and subsurface layers, respectively. During interdecadal evolutions, temperature and salinity anomalies tend to be of the opposite sign in the surface layer but of the same sign in the subsurface layer. Thus, they undergo out-of-phase changes in the surface layer (e. g., from

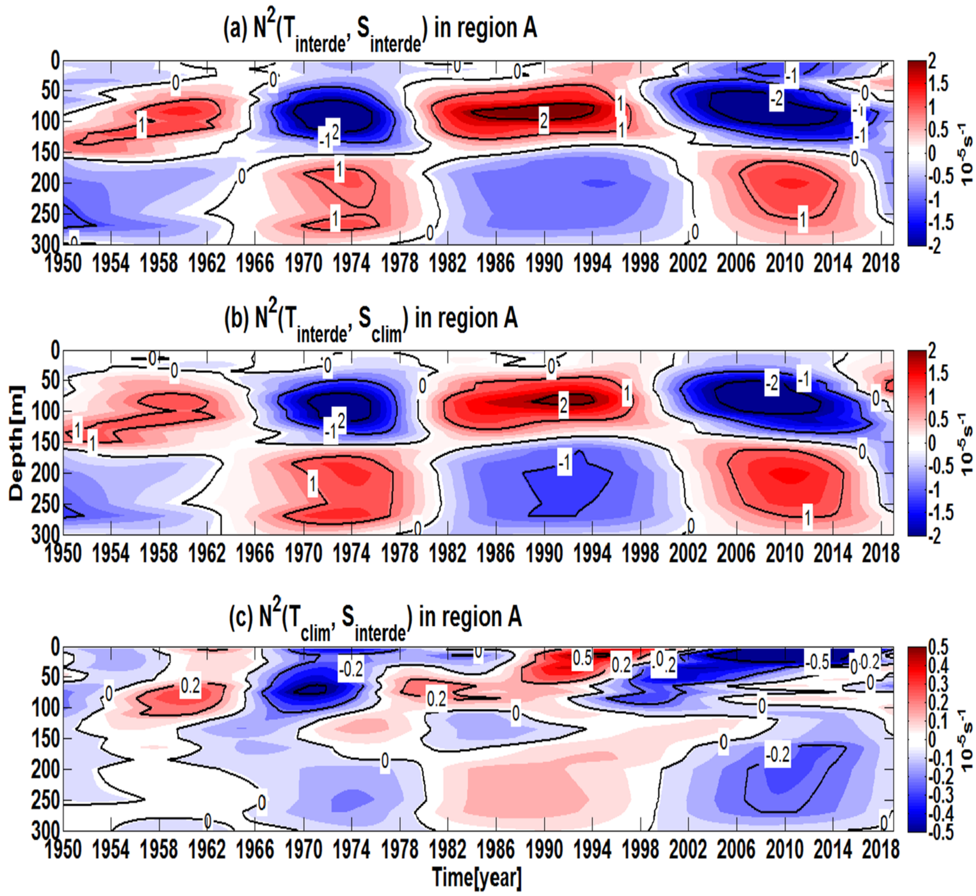

Fig. 13 The same as in Fig. 10 but for **a** $N^2(T_{interde}, S_{interde})$, **b** $N^2(T_{interde}, S_{clim})$, and **c** $N^2(T_{clim}, S_{interde})$, respectively. Note different color bar and contour are used in (**c**). The unit is 10^{-5} s^{-2} for N^2

positive SST anomalies and negative SSS anomalies to negative SST anomalies and positive SSS anomalies, respectively), but are nearly in-phase changes in the subsurface layers (e. g., from both positive temperature and salinity anomalies to both negative anomalies, respectively). Interdecadal evolution of temperature and salinity anomalies can be characterized by persistent and transitional phases in the upper ocean. During the 1980s-1990s, warm and fresh surface conditions persist in the western equatorial Pacific, which quickly transits into cold and salty conditions in the late 1990s. Then, cold and salty surface conditions persist in the 2000s and take another transition around in 2016–18, respectively.

Salinity exerts strong uncompensated and compensated effects on density respectively in the surface layer and subsurface layers, depending on the T–S relationships and their relative contributions during persistent and transitional phases. During interdecadal persistent phase, temperature anomalies are of the opposite sign in the surface and subsurface layers, whereas salinity anomalies are of the same sign uniformly in the upper ocean. During interdecadal transitional phase, temperature and salinity anomalies experience a transition coherently in the upper ocean. Correspondingly, salinity variability indicates obvious differences in its effects on density in the upper ocean. In the subsurface layers, salinity and temperature anomalies are nearly of the same sign and their effects are density-compensated, in which density anomalies are dominantly contributed from temperature, with weak effects of salinity. The situation is more complicated in the surface layer, where the salinity effects make an important contribution to density anomalies because temperature and salinity anomalies tend to have comparable effects. During the persistent phases, temperature and salinity anomalies are largely of the opposite sign, and so salinity effects are density-uncompensated, leading to enhanced density variability in the surface layer. During transitional periods, anomalies of SST, SSS and SSD are not in-phase, but have obvious differences in their sign transitions. One striking feature is that SSS and SST anomalies can be of

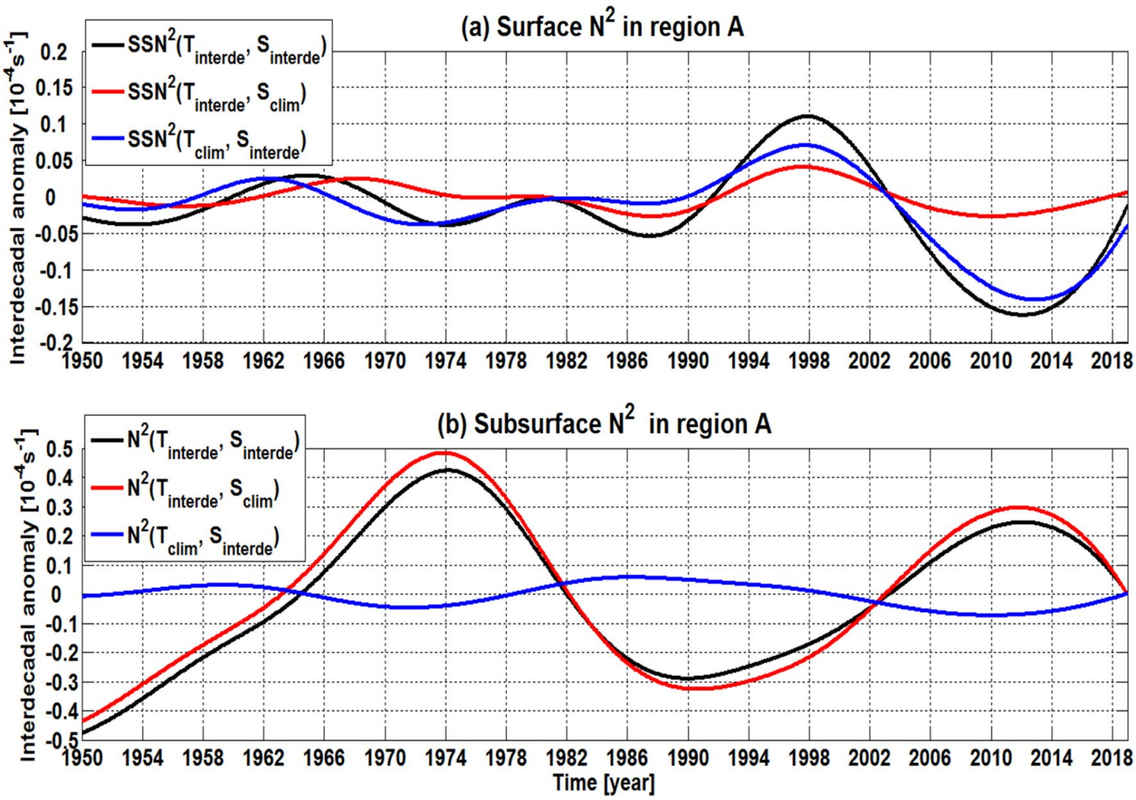

Fig. 14 The same as in Fig. 13 but for the corresponding time series of the three calculated N^2 fields at the sea surface (**a**) and at subsurface depth of 200 m (**b**). The unit is 10^{-5} s^{-2} for N^2

the same sign during the transitional periods, when salinity effect plays a dominant role in determining the sign of density anomalies. For example, the delayed sign transitions of density anomalies relative to temperature transition are caused by salinity anomalies. Evidently, salinity can be seen to have a delayed effect on the phase transitions of density variability.

The uncompensated and compensated salinity effects cause different consequences for changes in density and stratification during the persistent and transitional phases, respectively. Horizontally, for instance, the enhanced density anomalies due to uncompensated effects from salinity correspondingly produce large horizontal gradients of density and pressure. In contrast, compensated salinity effects contribute to suppressed density anomalies, which produce weak horizontal gradient of density and pressure. Relative to temperature effects, the asymmetric effects on density induced by salinity anomalies vertically in the surface layer and subsurface layers lead to a larger density contrast in the upper ocean, leading to larger changes in vertical stratification, which affects vertical mixing and SST stronger. So salinity variability can induce an enhancing effect on local SST in the western equatorial Pacific. Furthermore, the ways density is affected differently by salinity anomalies in the upper ocean leads to different consequences for SST modulations. As demonstrated in this study, there are obvious differences in the salinity-induced effect on local SST. In the case with uncompensated salinity effects, salinity anomalies induce an enhancing effect on local SST anomalies during persistent periods. In the case with compensated salinity effects, salinity anomalies can have a reducing effect on SST anomalies during transitional periods. As salinity can be important contributor to changes in density and stratification in the western equatorial Pacific, further diagnostic analyses are performed to clearly illustrate the relative contributions of temperature and salinity interdecadal anomalies to density and N^2. In particular, the signs of density and N^2 anomalies can be dominantly determined by salinity anomalies during transitional periods.

This paper presents preliminary results for salinity interdecadal variability and its effects in the western equatorial Pacific. Many related issues exist that remain to be addressed in the future. For example, the causes of salinity interdecadal variability in the western equatorial Pacific have not been presented in this paper. Indeed, many processes coexist in the region that can be responsible for it, including wind forcing, freshwater flux forcing and extratropical ocean influences. For instance, large changes in precipitation are observed over the western tropical Pacific (Yu and Weller 2007), which is closely related with the SPCZ (Kessler 1999). Also, salinity advections from the extratropical oceans are evident in the South Pacific (Luo et al. 2003, 2005; Zhang and Wang 2013) and in the North Pacific (Zhang and Levitus, 1997; Zhang and Liu 1999; Zhou and Zhang 2022). The roles of off-equatorial salinity anomalies and the SPCZ-induced direct freshwater flux forcing in salinity variability over the western equatorial Pacific are interesting topics, which needs to be addressed in the future.

The focus of this paper is on salinity variability and its effects on interdecadal time scale; many other time-scale signals coexist in the region (Fig. 3), including interannual variability associated with ENSO and trend. Previously, salinity interannual variability in the tropical Pacific and its effects have been examined extensively (Zhang et al. 2012; Zhi et al. 2015, 2019a, b). One important related issue here is the obvious interplays between interannual and interdecadal variabilities. As demonstrated in this study, salinity effects cause more stable stratification in the upper ocean of the western equatorial Pacific in the 1980s-1990s (correspondingly a warm and fresh interdecadal phase). This indicates an enhancing effect on SST anomalies, which is favorable for sustaining warm SST anomalies in the western-central equatorial Pacific. Note that this interdecadal warm and fresh period coincides with the frequent occurrence of more and stronger El Nino events (Zhang et al. 1998). So, salinity interdecadal variability may have influences on interannual variability in the tropical Pacific. The relationships between interannual and interdecadal variabilities and possible modulating effects of salinity interdecadal variability on ENSO in the region should be addressed in more details.

Appendix 1

This appendix presents some additional figures in support of arguments in the main texts (see Figs. 15, 16, 17, 18 19 and 20).

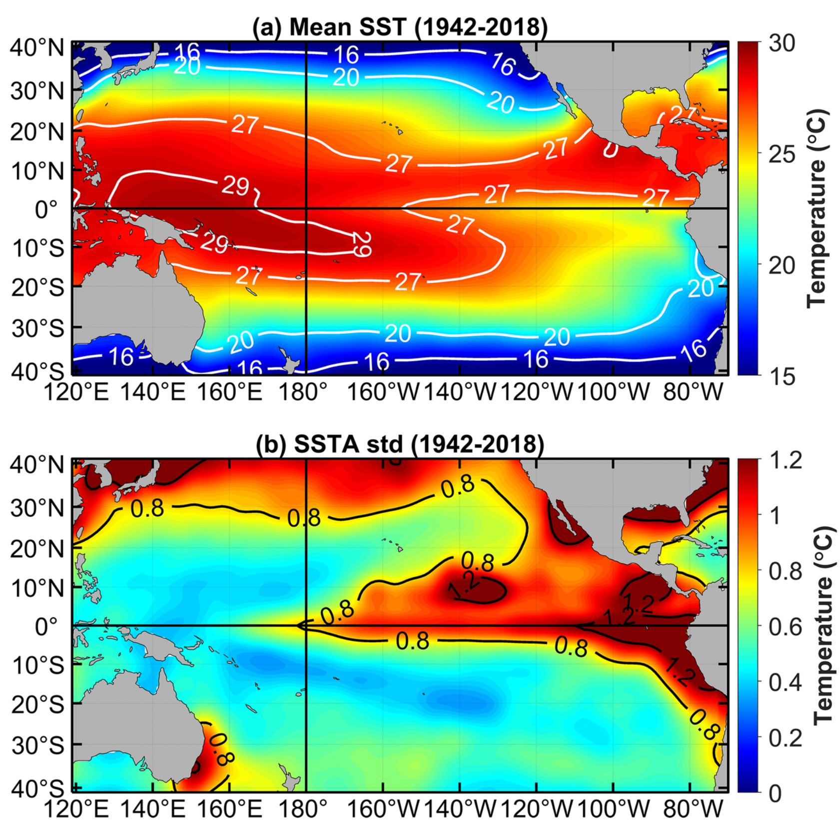

Fig. 15 Horizontal distribution of **a** climatological mean SST field and of **b** the standard deviation (STD) for SST interannual fields in the tropical Pacific, which is calculated from the reanalysis data during the period 1942–2018. The unit is °C

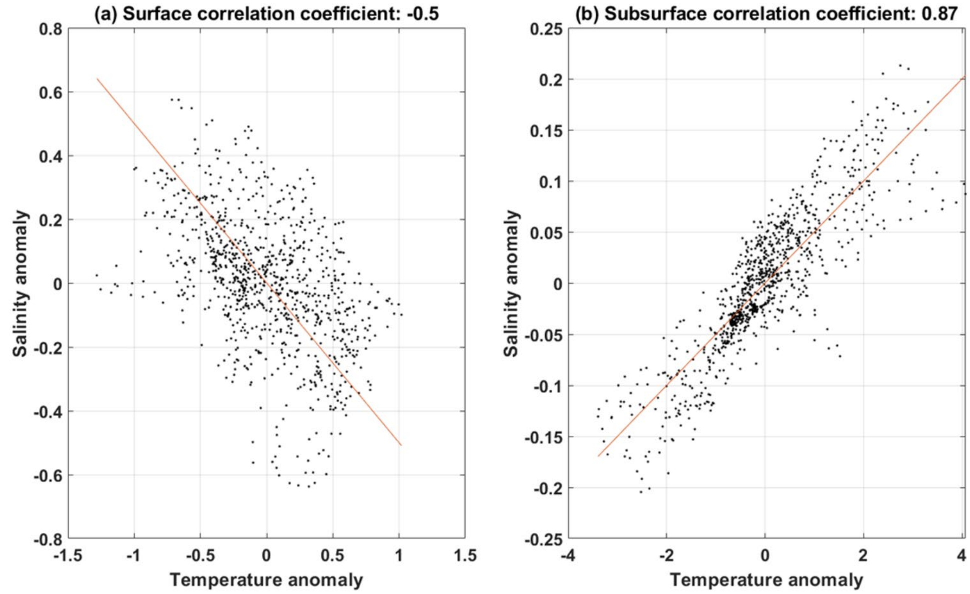

Fig. 16 a Scatter plot showing the relationship between SSTA and SSSA in the western equatorial Pacific (the region A as indicated in Fig. 1) and the corresponding correlation coefficient is − 0.50; **b** the same as in (**a**) but for subsurface temperature and salinity anomalies at depth of 200 m, and the corresponding correlation coefficient is 0.87

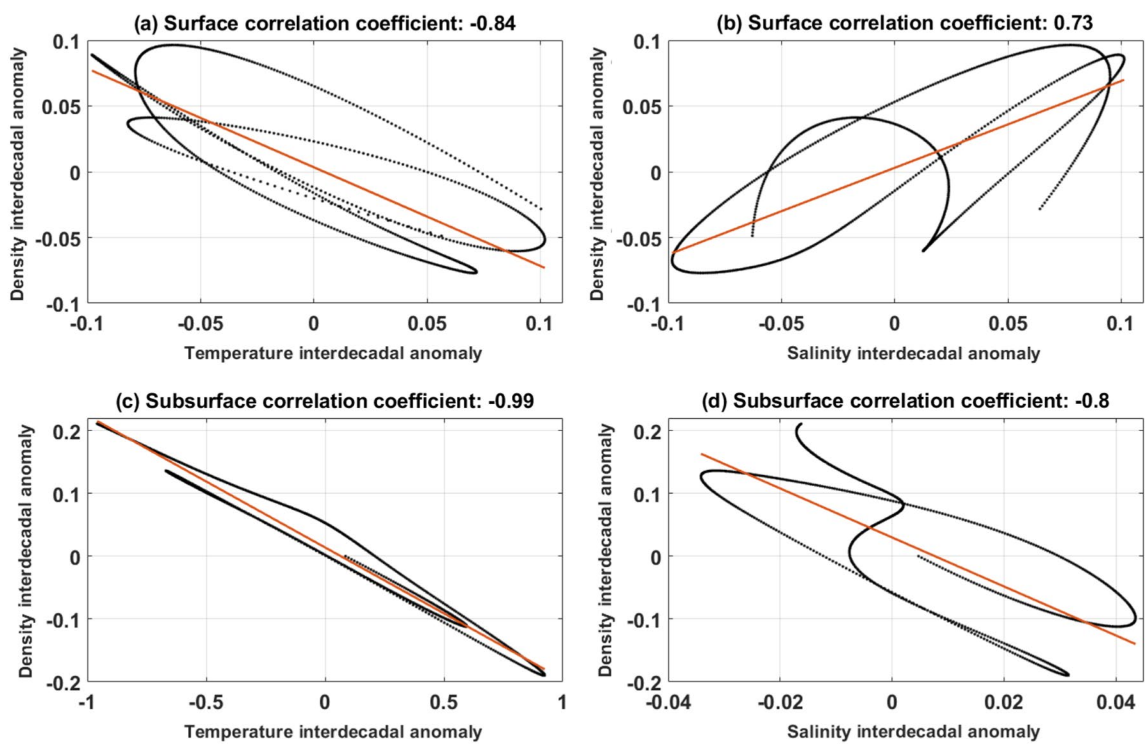

Fig. 17 **a** The relationship between density and temperature interdecadal anomalies at the sea surface in the region A with their correlation coefficient of − 0.84; **b** the same as in (**a**) but for density and salinity interdecadal anomalies with their correlation coefficient of 0.73; **c** the same as in (**a**) but for density and temperature interdecadal anomalies at depth of 200 m with their correlation coefficient of − 0.99; **d** the same as in (**c**) but for density and salinity interdecadal anomalies with their correlation coefficient of − 0.80

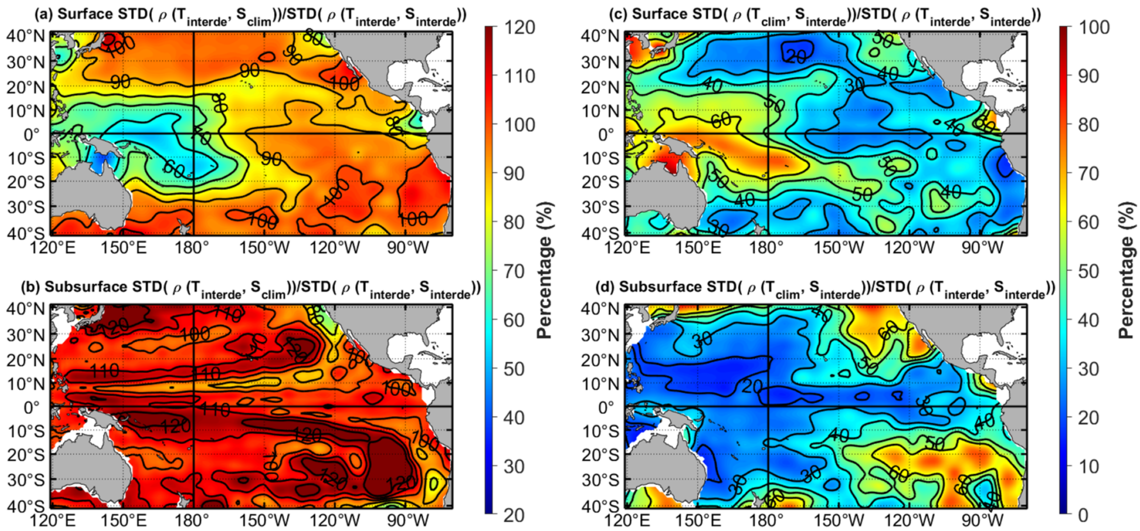

Fig. 18 The ratio of the standard deviation for interdecadal density anomalies; three calculations are performed to quantify individual contributions of temperature and salinity interdecadal fields to density (see the text for detail), $\rho(T_{interde}, S_{interde})$ is obtained using both interdecadal temperature and salinity fields; $\rho(T_{interde}, S_{clim})$ is obtained using interdecadal temperature field and climatological salinity field; $\rho(T_{clim}, S_{interde})$ is obtained using climatological temperature field and interdecadal salinity field, respectively: **a** $\rho(T_{interde}, S_{clim})/\rho(T_{interde}, S_{interde})$ at the surface; **b** $\rho(T_{interde}, S_{clim})/\rho(T_{interde}, S_{interde})$ at depth of 200 m; **c** $\rho(T_{clim}, S_{interde})/\rho(T_{interde}, S_{interde})$ at the surface; **d** $\rho(T_{clim}, S_{interde})/\rho(T_{interde}, S_{interde})$ at depth of 200 m

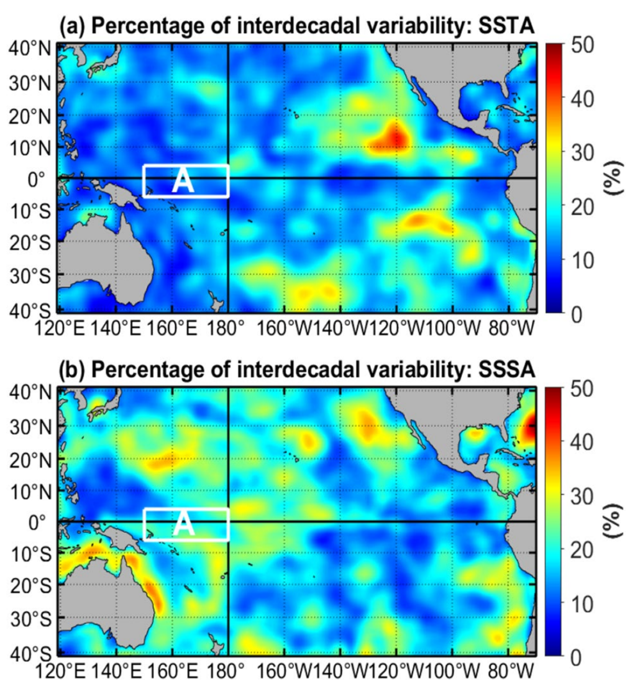

Fig. 19 The ratio of the standard deviations for SST (**a**) and SSS (**b**) interdecadal variabilities relative to those of total SST and SSS interannual variabilities

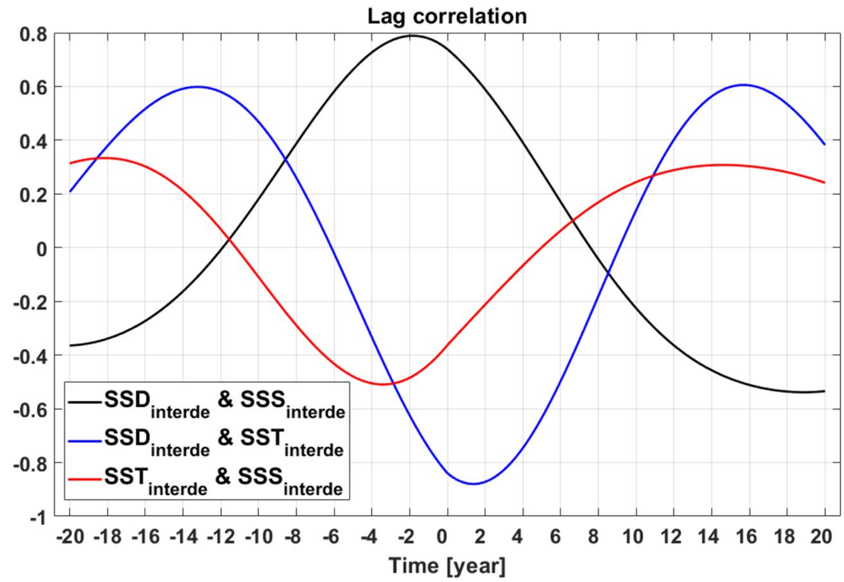

Fig. 20 The lagged correlation calculated among interdecadal anomalies of SSD, SST and SSS in the western equatorial Pacific (the region A as indicated in Fig. 1). Interdecadal anomalies of SSD lead SSS, with their maximum correlation coefficient being achieved (0.8) when the SSS is lagging the SSD by 2 years. Also, interdecadal anomalies of SSD lag SST, with their maximum correlation coefficient being achieved (− 0.83) when the SST is leading the SSD by 2 years; interdecadal anomalies of SST lead SSS, with their maximum correlation coefficient being achieved (− 0.5) when the SSS is lagging the SST by about 4 years

Acknowledgements The author wishes to thank the two anonymous reviewers for their numerous comments that helped improve the original manuscript significantly. The author would like to thank Dr. Zhaohua Wu for providing helps in using the EEMD method and the related Fortran code. Zhang is supported by the National Natural Science Foundation of China (NSFC; Grant No. 42030410) and the Startup Foundation for Introducing Talent of NUIST; Gao is supported by the Strategic Priority Research Program of the Chinese Academy of Sciences (CAS) (Grant Nos. XDA19060102, XDB42000000) and the NSFC (Grant No. 42176032); Wang is supported by the Strategic Priority Research Program of the CAS (Grant No. XDB40000000); Zhi and Wang are supported by the Financially supported by the Marine S&T Fund of Shandong Province for Pilot National Laboratory for Marine Science and Technology(Qingdao) (No. 2022QNLM010301-3 and 2022QNLM010301-4).

References

Cravatte S, Delcroix T, Zhang D, McPhaden M, Leloup J (2009) Observed freshening and warming of the western Pacific warm pool. Clim Dyn 33:565–589

Delcroix T (1998) Observed surface oceanic and atmospheric variability in the tropical Pacific at seasonal and ENSO timescales: a tentative overview. J Geophys Res 103:18611–18633. https://doi.org/10.1029/98JC0081482,32-43

Delcroix T, Picaut J (1998) Zonal displacement of the western equatorial Pacific “fresh pool.” J Geophys Res Oceans 103(C1):1087–1098

Delcroix T, Alory G, Cravatte S, Corrège T, Mcphaden MJ (2011) A gridded sea surface salinity data set for the tropical Pacific with sample applications (1950–2008). Deep Sea Res I 58(1):38–48

Du Y, Zhang Y, Shi J (2019) Relationship between sea surface salinity and ocean circulation and climate change. Sci China Earth Sci 62:771–782. https://doi.org/10.1007/s11430-018-9276-6

Feng L, Zhang R-H, Bo Yu, Han X (2020) The roles of wind stress and subsurface cold water in the second-year cooling of the 2017/18 La Niña event. Adv Atmos Sci 37:847–860. https://doi.org/10.1007/s00376-020-0028-4

Gao S, Qu T, Nie X (2014) Mixed layer salinity budget in the tropical Pacific Ocean estimated by a global GCM. J Geophys Res Oceans 119:8255–8270

Gao C, Zhang R-H, Karnauskas KB, Zhang L, Tian F (2020) Separating freshwater flux effects on ENSO in a hybrid coupled model of the tropical Pacific. Clim Dyn 54(11):4605–4626. https://doi.org/10.1007/s00382-020-05245-y

Good SA, Martin MJ, Rayner NA (2013) EN4: quality controlled ocean temperature and salinity profiles and monthly objective analyses with uncertainty estimates. J Geophys Res Oceans 118:6704–6716

Guan C, Hu S, McPhaden MJ et al (2019) Dipole structure of mixed layer salinity in response to El Niño-La Niña asymmetry in the tropical Pacific. Geophys Res Lett. https://doi.org/10.1029/2019GL084817

Hasson AEA, Delcroix T, Dussin R (2013) An assessment of the mixed layer salinity budget in the tropical Pacific Ocean: observations and modelling (1990–2009). Ocean Dyn 63:179–194

Hu S, Sprintall J (2016) Interannual variability of the Indonesian Throughflow: The salinity effect. J Geophys Res Oceans 121:2596–2615

Kang X, Huang R, Wang Z, Zhang R-H (2014) Sensitivity of ENSO variability to Pacific freshwater flux adjustment in the Community Earth System Model. Adv Atmos Sci 31(5):1009–1021. https://doi.org/10.1007/s00376-014-3232-2

Kang X, Zhang R-H, Wang GS (2017) Effects of different freshwater flux representations in an ocean general circulation model of the tropical pacific. Sci Bull 62:345–351. https://doi.org/10.1016/j.scib.2017.02.002

Kessler WS (1999) Interannual variability of the subsurface high salinity tongue south of the equator at 165°E. J Phys Oceanogr 29(8):2038–2049

Li Y, Wang F, Han W (2013) Interannual sea surface salinity variations observed in the tropical North Pacific Ocean. Geophys Res Lett 40:2194–2199. https://doi.org/10.1002/grl.50429

Lukas R, Lindstrom E (1991) The mixed layer of the western equatorial Pacific Ocean. J Geophys Res 96:3343–3357

Luo J-J, Masson S, Behera SK, Delecluse P, Gualdi S, Navarra A, Yamagata T (2003) South Pacific origin of the decadal ENSO-like variation as simulated by a coupled GCM. Geophys Res Lett 30(24):2250. https://doi.org/10.1029/2003GL018649

Luo Y, Rothstein LM, Zhang R-H, Busalacchi AJ (2005) On the connection between South Pacific subtropical spiciness anomalies and decadal equatorial variability in an ocean general circulation model. J Geophys Res 110:C10002. https://doi.org/10.1029/2004JC002655
Maes C (2000) Salinity variability in the equatorial Pacific Ocean during the 1993-98 period. Geophys Res Lett 27(11):1659–1662
Maes C, Ando K, Delcroix T, Kessler WS, McPhaden MJ, Roemmich D (2006) Observed correlation of surface salinity, temperature and barrier layer at the eastern edge of the western Pacific warm pool. Geophys Res Lett 33(6):L06601. https://doi.org/10.1029/2005GL024772
McDougall TJ, Jackett DR, Millero FJ, Pawlowicz R, Barker PM (2012) A global algorithm for estimating absolute salinity. Ocean Sci 8:1123–1134. https://doi.org/10.5194/os-8-1123-2012
Miller JR (1976) The salinity effect in a mixed-layer ocean model. J Phys Oceanogr 6:29–35
Picaut J, Ioualalen M, Menkès C, Delcroix T, Mcphaden MJ (1996) Mechanism of the zonal displacements of the Pacific warm pool: Implications for ENSO. Science 274(5292):1486–1489
Qi J, Zhang L, Qu T, Yin B, Xu Z, Yang D, Qin Y (2019) Salinity variability in the tropical Pacific during the Central-Pacific and Eastern-Pacific El Niño events. J Mar Syst 199:103225
Qu T, Song YT, Maes C (2014) Sea surface salinity and barrier layer variability in the equatorial Pacific as seen from Aquarius and Argo. J Geophys Res Oceans 119:15–29
Sasaki YN, Schneider N, Maximenko N, Lebedev K (2010) Observational evidence for propagation of decadal spiciness anomalies in the North Pacific. Geophys Res Lett 37:L07708. https://doi.org/10.1029/2010GL042716
Schneider N (2000) A decadal spiciness mode in the tropics. Geophys Res Lett 27:257–260. https://doi.org/10.1029/1999GL002348
Singh A, Delcroix T, Cravatte S (2011) Contrasting the flavors of El Niño-Southern Oscillation using sea surface salinity observations. J Geophys Res Oceans 116(C6):C06016. https://doi.org/10.1029/2010jc006862
Vialard J, Delecluse P, Menkes C (2002) A modeling study of salinity variability and its effects in the tropical Pacific Ocean during the 1993–1999 period. J Geophys Res 107(C12):8005. https://doi.org/10.1029/2000JC000758
Vinogradova NT, Ponte RM (2013) Clarifying the link between surface salinity and freshwater fluxes on monthly to interannual time scales. J Geophys Res Oceans 118:3190–3201. https://doi.org/10.1002/jgrc.20200
Wu Z, Huang NE, Long SR, Peng CK (2007) On the trend, detrending, and variability of nonlinear and nonstationary time series. Proc Natl Acad Sci 104(38):14889–14894
Wu Z, Feng J, Qiao F, Tan ZM (2016) Fast multidimensional ensemble empirical mode decomposition for the analysis of big spatio-temporal datasets. Phil Trans R Soc A 374:20150197
Yu L, Weller RA (2007) Objectively analyzed air–sea heat fluxes for the global ice-free oceans (1981–2005). Bull Am Meteorol Soc 88:527–539
Zhang R-H, Busalacchi AJ (2009) Freshwater flux (FWF)-induced oceanic feedback in a hybrid coupled model of the tropical Pacific. J Clim 22:853–879
Zhang R-H, Levitus S (1997) Structure and cycle of decadal variability of upper ocean temperature in the North Pacific. J Clim 10:710–727
Zhang R-H, Liu Z (1999) Decadal thermocline variability in the North Pacific Ocean: two anomaly pathways around the subtropical gyre. J Clim 12:3273–3296
Zhang R-H, Wang Z (2013) Model evidence for interdecadal pathway changes in the subtropics and tropics of the South Pacific Ocean. Adv Atmos Sci 30(1):1–9. https://doi.org/10.1007/s00376-012-2048-1
Zhang R-H, Rothstein LM, Busalacchi AJ (1998) Origin of upper-ocean warming and El Niño change on decadal scales in the tropical Pacific Ocean. Nature 391:879
Zhang R-H, Wang G-H, Chen D, Busalacchi AJ, Hackert EC (2010) Interannual biases induced by freshwater flux and coupled feedback in the tropical Pacific. Mon Wea Rev 138:1715–1737
Zhang R-H, Zheng F, Zhu JS, Pei YH, Zheng QA, Wang ZG (2012) Modulations of El Niño-Southern oscillation by climate feedbacks associated with freshwater flux and ocean biology in the tropical Pacific. Adv Atmos Sci 29(4):647–660
Zhang R-H, Gao C, Feng L (2022) Recent ENSO evolution and its real-time prediction challenges. National Sci Rev. https://doi.org/10.1093/nsr/nwac052
Zheng F, Zhang R-H (2012) Effects of interannual salinity variability and freshwater flux forcing on the development of the 2007/08 La Niña event diagnosed from Argo and satellite data. Dyn Atmos Oceans 57:45–57
Zheng F, Zhang R-H (2015) Interannually varying salinity effects on ENSO in the tropical Pacific: a diagnostic analysis from Argo. Ocean Dyn 65(5):691–705
Zhi H, Zhang R-H, Lin P, Wang L, Yu P (2015) Quantitative analysis of the feedback induced by the freshwater flux in the tropical Pacific using CMIP5. Adv Atmos Sci 32:1341–1353. https://doi.org/10.1007/s00376-015-5064-0
Zhi H, Zhang R-H, Lin PF, Yu P (2019a) Interannual salinity variability in the tropical Pacific in CMIP5 simulations. Adv Atmos Sci 36(4):378–396. https://doi.org/10.1007/s00376-018-7309-1
Zhi H, Zhang R-H, Lin P, Shi S (2019b) Effects of salinity variability on recent El Niño events. Atmosphere 10:475–480. https://doi.org/10.3390/atmos10080475
Zhou GH, Zhang R-H (2022) Structure and evolution of decadal spiciness variability in the North Pacific during 2004–20, revealed from Argo observations. Adv Atmos Sci. https://doi.org/10.1007/s00376-021-1358-6
Zhu J, Huang B, Zhang R-H, Hu Z-Z, Kumar A, Balmaseda MA, Kinter JL III (2014) Salinity anomaly as a trigger for ENSO events. Sci Rep 4:6821. https://doi.org/10.1038/srep06821